J. Plasma Phys. (2023), *vol*. 89, 905890302 © The Author(s), 2023.
Published by Cambridge University Press
doi:10.1017/S0022377823000387

Lane formation in 3D driven pair-ion plasmas: II Non-Parallel External Forcing

Vishal Kumar Prajapati [1], **Swati Baruah** [1,†] **and Rajaraman Ganesh** [2]

[1]Department of Physics, School of Basic Sciences, The Assam Kaziranga University, Jorhat 785006, Assam, India

[2]Institute for Plasma Research, Bhat, Gandhinagar 382428, Gujarat, India

(Received 20 October 2022; revised 4 April 2023; accepted 4 April 2023)

In Part 1 of the companion paper, we have investigated lane formation dynamics of driven three-dimensional (3-D) pair-ion plasmas (PIP) in the presence of parallel external forcing using extensive Langevin dynamics (LD) simulation. In continuation of the work, in this Part 2, we investigate lane formation dynamics in the presence of non-parallel external forcing, and the effect of both constant and time varying forces are studied. In our model, positively charged PIP particles are pushed into the field direction by an external force $\boldsymbol{F}_A = E_A \cos \omega_A t$ while the negatively charged PIP particles are pulled by an external force $\boldsymbol{F}_B = E_B \cos \omega_B t$ in a direction perpendicular to the external force $\boldsymbol{F}_A$. We show that in the case of non-parallel forces, the lanes are observed with an orientation (characterised by angle of inclination θ) tilted in the direction of the force difference vector $(\boldsymbol{F}_A - \boldsymbol{F}_B)$. The instantaneous lane order parameter, order parameter with gradient of angle of inclination $(\phi(\theta))$ and distribution function of $\Delta\theta$ have been implemented to characterise the phase transition. A spontaneous formation and breaking of lanes are observed when under the influence of time-varying forces. The effect is further investigated for three different situations: first, when $\omega_A \neq 0$ and $\omega_B = 0$; second, when $\omega_A = \omega_B \neq 0$; and third, for $\omega_A \neq \omega_B \neq 0$. Our study reveals that for the first case, a periodic oscillation of angle of inclination is observed. If oscillating forces of the same frequency are applied, the oscillation in angle of inclination disappears, and spontaneous formation and breaking of lanes is observed. However, in the presence of forces with different frequencies, flipping of lane inclination between the positive and negative domain of θ is observed. Further, some aspects of the lane formation dynamics of a PIP system is also studied in the presence of an external magnetic field where the lane formation dynamics is found to be accelerated.

Keywords: plasma simulation, strongly coupled plasmas

1. Introduction

In recent studies, we have analysed the occurrence of lane formation in a two-dimensional (2-D) pair-ion plasma (PIP) system using Langevin dynamics (LD) simulation both in the presence (Baruah, Sarma & Ganesh 2021*b*) and absence (Sarma, Baruah & Ganesh 2020) of an external magnetic field. A simulation by Baruah, Prajapati & Ganesh (2021*a*) was also reported addressing the effect of obstacle and geometric

† Email address for correspondence: baruah.s1@gmail.com

aspect ratio on lane formation dynamics for a 2-D PIP system. On this ubiquitous lane formation phenomenon, several simulation (Dzubiella, Hoffmann & Löwen 2002; Glanz & Löwen 2012) and experimental (Leunissen *et al.* 2005; Hynninen *et al.* 2006) studies have also been reported on various systems. Most of the studies stated above are carried out on 2-D systems. However, most laboratory and natural plasma systems are three-dimensional (3-D) in nature, which could provide a much richer scenario on phase transition phenomena. Hence, an obvious next step is to study the lane dynamics in a 3-D set-up for its relevance to real-life situations.

Patterns are fascinating phenomena with a clear degree of regularity. Analysing patterns is crucial in identifying the controlling parameters and making an attempt to understand the criteria for transitions between different phases. The study of lane formation where the system exhibits various structures is not only crucial for a better understanding of the nature from a fundamental point of view, but also its relevance to emerging technological contexts ranging from nanoscience and material synthesis (Ostrikov, Cvelbar & Murphy 2011) to water activation (Traylor *et al.* 2011) and medicine (Kong *et al.* 2009). In some plasma process, these structures could be desirable, adding to the outcome of the processes like surface texturization, whereas in some processes, it could be detrimental and hence undesirable when it produces non-uniformity or electrode erosion (Lichtenberg *et al.* 2002; Yang & Heberlein 2007). For example, in liquid mixing processes (Podvigina 2006), the recirculation flow pattern is very much desirable, whereas local heating or cooling produced by thermal spots could impact the final outcome in surface treatments (Bruggeman & Leys 2009; Trelles 2013). Thus, the study of lane formation could prove to be crucial for technological applications that either mitigate or exploit this behaviour of lane formation.

In Part 1 of the companion paper (Prajapati, Baruah & Ganesh 2023), we have extensively discussed the influence of parallelly applied external electric field forces on the behaviour of lane dynamics on a 3-D PIP system, which, to the best of our knowledge, has never been addressed before. In the present work (i.e. Part 2), we report an investigation of the same phenomena in a 3-D PIP system in the presence of non-parallel external forces with various field strength values for the inertial limit when the system is underdamped and, hence, the particles can accelerate (i.e. $m_i \mathrm{d}^2 r_i/\mathrm{d}t^2 \neq 0$; (1.1) mentioned below). This limit becomes possible for lower background damping or a smaller value of γ. Further, the effect of an external magnetic field on the dynamics of lanes is also studied. Physically, non-parallel forcing can be realised by the crossing of two external fields, e.g. laser optical with electric, laser optical with magnetic, gravity with electric etc. The existence of vortices is also predicted for plasmas immersed in crossed magnetic and gravitational fields (Aburdzhaniia *et al.* 1984). Crossed beam configurations are also used for plasma confining and controlling the plasma position (Sun & Alwahabi 2022). However, electric and magnetic fields are used for this study.

To carry out the study, we performed extensive LD simulation using the OpenMP parallel program. In our model, we consider N charged particles of equal mass having charge anti-symmetry inside a cubic box having size $L_x = L_y = L_z = L$. We solve the Langevin equation of motion given by

$$m_i \frac{\mathrm{d}^2 \boldsymbol{r}_i}{\mathrm{d}t^2} = -\gamma \frac{\mathrm{d}\boldsymbol{r}_i}{\mathrm{d}t} - \sum_{i<j} \boldsymbol{\nabla} U\left(r_{ij}\right) + \boldsymbol{F}_{\mathrm{ext}} + \boldsymbol{F}_i^{(R)}. \tag{1.1}$$

There are different forces experienced by the PIP particles: first, there is the force due to background dampening, then there is the force attributed to the interparticle interactions due to the Yukawa-like interaction potential, then there is the external forcing mainly

https://doi.org/10.1017/S0022377823000387 Published online by Cambridge University Press

non-parallel electric ($\boldsymbol{F}_E$) and magnetic forces ($\boldsymbol{F}_{\rm mag}$) which are modelled through the term $\boldsymbol{F}_{\rm ext}$ such that $\boldsymbol{F}_E = \boldsymbol{F}_A$ for positively charged particles and $\boldsymbol{F}_E = \boldsymbol{F}_B$ for negatively charged particles. Here, $\boldsymbol{F}_i^{(R)}$ is the random kicks experienced by the particles from the background 'bath'.

We solve (1.1) for the system using a Velocity Verlet integrator in the presence of non-parallel external forces. Here, the entire work is performed for κ=10^{-4}, where $\kappa = a/\lambda_D$ is the screening parameter resulting from the shielding dynamics of 'background' charged particles (Sarma *et al.* 2020), λ_D is the Debye length and 'a' is the Wigner–Seitz radius; for the rest of the presentation, this is the value of κ used. Forces due to particle interactions are calculated using simple truncation of the interaction potential. We do not employ the Ewald sum, as the Ewald contribution towards potential energy is very small and hence neglected. We study the case where the two external forces are not parallel. Force $\boldsymbol{F}_A$ is applied in the z-direction, while $\boldsymbol{F}_B$ is applied in the x-direction, i.e. the force due to external electric field $\boldsymbol{F}_E$ is different for both halves of the particles. It is $\boldsymbol{F}_E = \boldsymbol{F}_A$ for positively charged particles and $\boldsymbol{F}_E = \boldsymbol{F}_B$ for negatively charged particles. In both the cases, the field free thermodynamic equilibrium state is a mixed fluid state. The lane formation is then detected and analysed both in the presence and absence of an external magnetic field. The rest of the fine details of the model and simulation procedure are discussed in Part 1 of the companion paper (Prajapati *et al.* 2023).

The rest of the paper is organised as follows. In § 2, we present the diagnostic techniques, i.e. order parameter with gradient of ϕ and distribution function of $\Delta\theta$. The results for non-parallel forces follow, both in the presence and absence of an external magnetic field, and these are presented and discussed in detail in § 3. Particularly, in § 3.1, the results in the presence of constant external non-parallel forces are presented and in § 3.2, the results in the presence of time varying external non-parallel forces are presented. Finally, we finish with the conclusions in § 4.

2. Simulation procedure

2.1. *Order parameter with a gradient of* θ ($\phi(\theta)$)

In the application of two non-parallel external electric field forces ($\boldsymbol{F_A}$, $\boldsymbol{F_B}$), tilted lanes are observed to form (details are discussed in § 3) in our PIP system. The lanes thus formed are inclined with a characteristic angle of inclination 'θ' in a direction along the resultant of the two non-parallel forces $\boldsymbol{F}_A$ and $\boldsymbol{F}_B$ which is calculated using the following equation:

$$\theta = \tan^{-1}\frac{F_A}{F_B}. \tag{2.1}$$

For the scope of the study, θ is measured in degrees. If the applied electric field is oscillatory, θ proves to be time varying in nature. However, in the presence of a constant electric field, θ remains constant throughout the simulation runs. The order parameter is measured by dividing the 3-D system into $n_{\rm div}$ number of grids along the characteristic angle of inclination (θ). The order parameter of the system along θ is then defined as

$$\phi = \left\langle \frac{1}{n_{\rm div}} \sum_{k=1}^{n_{\rm div}} |\phi_k| \right\rangle, \tag{2.2}$$

where ϕ_k is the order parameter of the kth grid given by $\phi_k = (n_k^+ - n_k^-)/(n_k^+ + n_k^-)$. Generally, following this method (Prajapati *et al.* 2023), the instantaneous order parameter ϕ is measured along any one particular direction of inclination of the lanes (i.e. for a fixed value of θ). However, for the non-parallel time-varying electric field case, the

https://doi.org/10.1017/S0022377823000387 Published online by Cambridge University Press

measurement of the order parameter along any one particular direction would not be a correct measure of orderness for the system under study. Depending on θ, the angle along which the order parameter is measured also changes periodically. Therefore, in this sub-section, a diagnostic technique, the order parameter with gradient of θ, i.e. $\phi(\theta)$, is introduced to measure the value of the order parameter when tilted lanes are formed in the PIP system on application of non-parallel forces. In this method, the order parameter at any instant of time t is measured using (2.2), where, the direction of measurement is along θ, calculated using (2.1). While taking the next measurement at the $(t + \delta t)$ time step, the direction of measurement is again changed in accordance with (2.1), and the order parameter corresponding to this new direction is again measured using (2.2). This change is maintained throughout the simulation run which results in an order parameter plot where an oscillating gradient of θ exists along the time axis. However, θ becomes constant which gives a fixed orientation of the lane in the presence of non-parallel constant electric fields. Thus, this diagnostic technique ensures that the order parameter is always measured in the direction parallel to the direction of lane formation which is critical to diagnose the lane or no lane state.

2.2. *Distribution function of* $\Delta\theta$

The fluctuations associated with the measurement of angle of inclination (θ) of the lanes need to be quantified for a better understanding of the parameter θ. To do so, a new diagnostic technique is introduced in this sub-section to construct the distribution of $\Delta\theta$. Initially, the mean of θ, i.e. ($\bar{\theta}$), is obtained over a fixed interval of time 't' followed by obtaining

$$\Delta\theta(t) = \theta(t) - \bar{\theta}. \tag{2.3}$$

The distribution curve of $\Delta\theta$ is then obtained by plotting $\Delta\theta$ against the counts or number of occurrences of each individual $\Delta\theta$ value. This curve thus helps in resolving the fluctuation in the time variation of the θ plot in turn reducing the noise in the simulation data obtained for the measurement of θ. The distribution can be characterised on the basis of being a Gaussian or non-Gaussian distribution to study the mean, standard deviations and skewness of the distribution of the curve to obtain useful information. It is expected that the θ values recorded during simulation will tend to have very few instances where they differ from the mean value for the complete simulation run given.

3. Results and discussions

In this section, we mainly focus on the results obtained for the study of non-equilibrium lane formation dynamics in a 3-D PIP system for the inertial (or finite mass 'm') or underdamped case in the application of non-parallel external forces. Here, the effect of both constant ($\omega_A = \omega_B = 0$) and oscillatory ($\omega_A \neq 0$ and $\omega_B \neq 0$) external electric forces are observed in the presence ($\beta \neq 0$) and absence ($\beta = 0$) of the external magnetic field. Here, ω_A and ω_B represent the frequencies associated with $\boldsymbol{F}_A$ and $\boldsymbol{F}_B$, respectively.

3.1. *Constant electric fields*

In this sub-section, we show that lane formation occurs in the presence of non-parallel forces which are constant in nature, both in the presence ($\beta \neq 0$) and absence ($\beta = 0$) of an external magnetic field. Here, positively charged PIP particles are drifting in the z-direction with force $\boldsymbol{F}_A$, while the negatively charged PIP particles are drifting in the x-direction with force $\boldsymbol{F}_B$. The other parameters are fixed to $\Gamma = 2.5$, $\rho = 0.245$ and $\omega_A = \omega_B = 0$.

https://doi.org/10.1017/S0022377823000387 Published online by Cambridge University Press

In figure 1(*a*), running ϕ as a function of $t\omega_{pd}$ is plotted during the simulation period and the corresponding snapshots for the instantaneous positions of the PIP particles are represented in figure 1(*b*). The magnitude of the forces used are $\boldsymbol{F}_A = 200$ and $\boldsymbol{F}_B = 100$, and the study is performed in the absence of an external magnetic field, i.e. $\beta = 0$. In our study, the system is first equilibrated to the desired temperature for $t\omega_{pd} = 600$ step, which initially corresponds to a homogeneous completely mixed state as shown in the first snapshot recorded at the $t\omega_{pd} = 54$ step in figure 1(*b*). After some time interval, a row-like arrangement of particles is developed at the $t\omega_{pd} = 270$ step by the PIP particles similar to that observed in Part 1 of the companion paper (figure 2 of Part 1 Prajapati *et al.* 2023). For more clarity, the (i) 3-D view, (ii) view along the x–z plane, (iii) view along the y–z plane and (iv) top view of the simulation chamber recorded at the $t\omega_{pd} = 270$ step are also shown in figure 1(*c*). Here, the non-parallel external electric forces with perpendicular directions are applied at the $t\omega_{pd} = 600$ step. It is observed that on sudden application of the external forces, structures are broken down to a mixed random state followed gradually by the tilted lanes. Results are presented in figure 1(*b*): tilted lane formation is clearly visible in the plane spanned by the two forces $\boldsymbol{F}_A$ and $\boldsymbol{F}_B$, and corresponding snapshots recorded at the $t\omega_{pd} = 648, 1620$ time steps are presented. For this study, as mentioned above, we have calculated a suitable order parameter ϕ which is sensitive to tilted lane formation, as indicated in figure 1(*a*). The order parameter, when measured in the direction parallel to the lanes, exhibits a jump beyond $\phi = 0.5$, indicating a tilted lane formation (see figure 1*b*). The physical reason for the formation of tilted lanes may be understood as follows. It is well known that non-parallel forces can be realised by the crossing of two external fields, e.g. gravity with electric, laser optical with electric, laser optical with magnetic etc. In this study, it is incorporated by using two external electric fields (both constant and oscillatory). The + and − species of PIP generally respond differently to the two external electric fields such that the resulting total external force will be different and in the direction along which tilted lanes form.

The electric fields strengths have a significant effect on the orientation of the lanes, which is checked by observing the angle of inclination (θ) of the lanes with the x-axis for different values of the ratio between the applied external forces, i.e. $\boldsymbol{F}_r = \boldsymbol{F}_A/\boldsymbol{F}_B$. In support of this observation, in figure 2(*a*), the simulation snapshots are recorded at the end of every simulation run for different values of $F_r = 0.57$, 1.0, 2.0 and 2.5. This variation of $\boldsymbol{F}_r$ is recorded by varying the magnitude of $\boldsymbol{F}_B$ as 80, 100, 200 and 350, keeping the other force $\boldsymbol{F}_A$ fixed at 200. Our study reveals that the angle of inclination made with the positive x-axis is seen to be reduced with decreasing $\boldsymbol{F}_r$. In addition, the lane thickness also reduces as $\boldsymbol{F}_r$ is decreased. For each simulation snapshot in figure 2(*a*), the time variation of θ is measured by calculating the direction along which ϕ is maximum. It is obvious to assume that the orderness when measured parallel to the lane will be maximum, as compared to that with any other direction of measurement. This property is exploited to determine the direction along which ϕ is maximum at any instant of time. Performing this measurement throughout the simulation, the corresponding time variation of θ is obtained, which is shown in figure 2(*b*). Here, the measurement of θ is done after the application of the external non-parallel forces $\boldsymbol{F}_A$ and $\boldsymbol{F}_B$. A constant angle of inclination is found throughout the simulation run and θ grows with increasing $\boldsymbol{F}_r$ value. Upon investigating, it is found that the angle of inclination values obtained from simulation for different values of $\boldsymbol{F}_r$ are consistent with (2.1). In figure 2(*c*), the distribution function of $\Delta\theta$ is plotted for the same values of F_r as stated above. The distribution of $\Delta\theta$ is found to be almost Gaussian in nature where the mean, median and mode of an individual distribution are the same. It is observed that with increasing F_r, the width of the distribution curve also increases. It is also observed that the curve is centrally symmetric and not skewed. The

https://doi.org/10.1017/S0022377823000387 Published online by Cambridge University Press

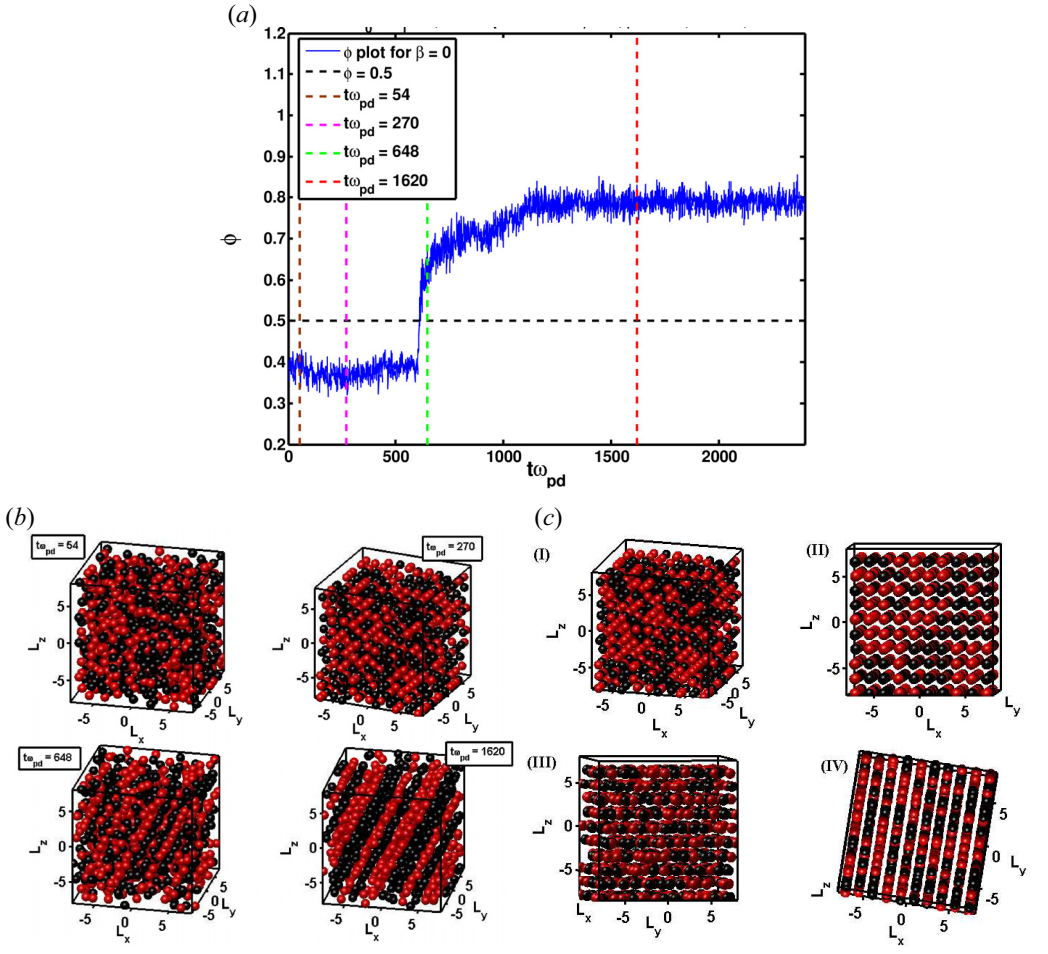

FIGURE 1. (*a*) Order parameter ϕ versus $t\omega_{pd}$ plot of the 3-D PIP system with perpendicular external fields. (*b*) Typical simulation snapshots recorded at $t\omega_{pd} = 54, 270, 648, 1620$ time steps. (*c*) View of the snapshot from different angles recorded at the $t\omega_{pd} = 270$ step: (i) 3-D view; (ii) view along the x–z plane; (iii) view along the y–z plane; (iv) top view. Here, half of the PIP particles are drifting in the z-direction with force $\boldsymbol{F}_A = 200$, while the other half of the PIP particles are drifting in the x-direction with force $\boldsymbol{F}_B = 100$. The other parameters used are $\Gamma = 2.5$, $\rho = 0.245$ and $\omega_A = \omega_B = 0$.

peak at $\Delta\theta = 0$ indicates that the fluctuations in θ are more centred towards $\bar{\theta}$. Thus, $\bar{\theta}$ is a good approximation of the angle of inclination (θ) for the particular case. The angle of inclination is also measured in the presence of an external magnetic field ($\beta \neq 0$), and the results are compared with those obtained using (2.1) along with the results for the $\beta = 0$ case as shown in figure 3. From the figure, in the absence of a magnetic field ($\beta = 0$), the θ values exhibited by the system are consistent with the values predicted by (2.1). However, when a magnetic field is present ($\beta = 1.0$), the curve starts to deviate from the theoretical curve at higher F_r values. Thus, the magnetic field clearly has some influence on the angle of inclination of the lanes which demands further refinement of (2.1) by incorporating a magnetic field term (which is not done here).

https://doi.org/10.1017/S0022377823000387 Published online by Cambridge University Press

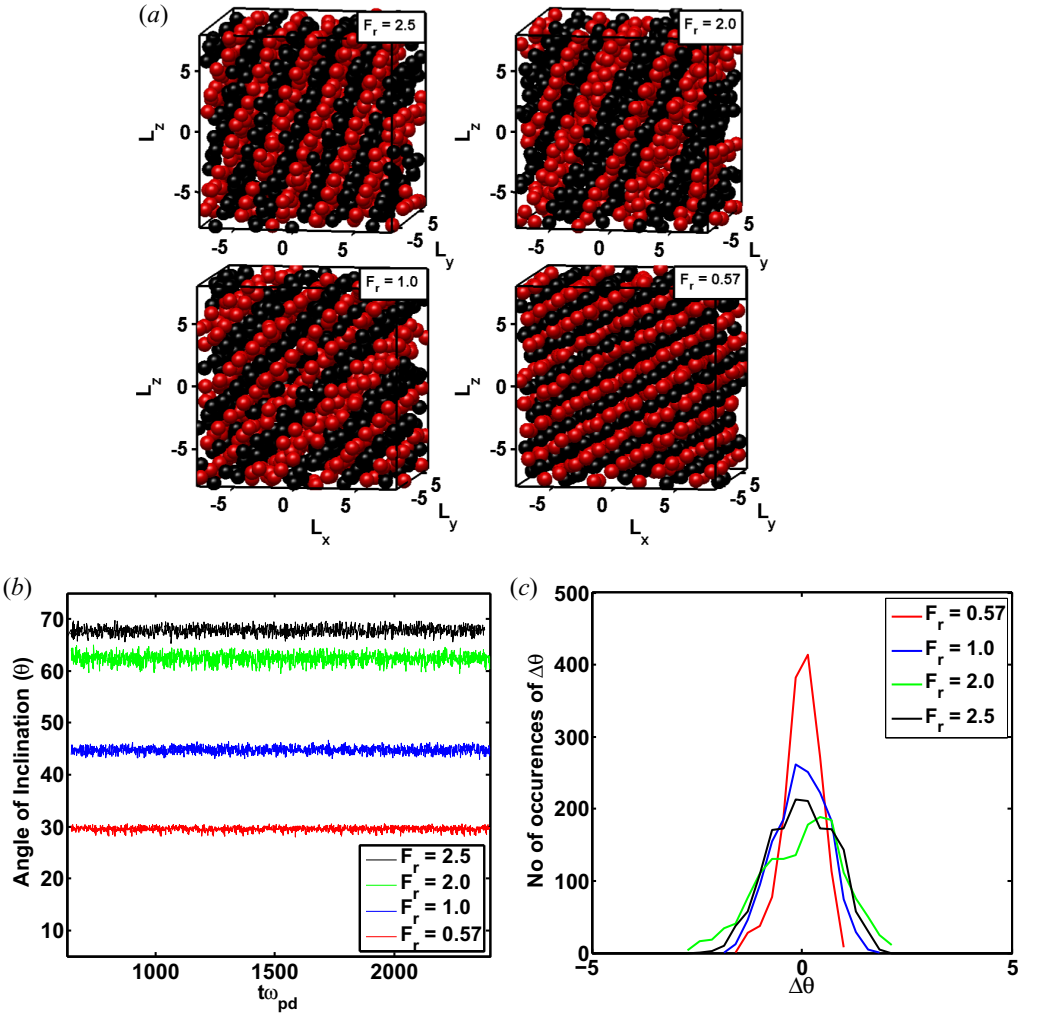

FIGURE 2. (*a*) Typical simulation snapshots of the 3-D PIP system indicating the formation of tilted lanes with perpendicular fields. (*b*) Angle of inclination versus $t\omega_{pd}$ plot of the 3-D PIP system with perpendicular fields. (*c*) Distribution function of $\Delta\theta$ (in degrees) for different F_r values. The positively charged PIP particles are drifting in the z-direction, while negatively charged particles are drifting in the x-direction and $\boldsymbol{F}_r = \boldsymbol{F}_A/\boldsymbol{F}_B = 0.57,\ 1.0,\ 2.0,\ 2.5$. The snapshots are recorded at $t\omega_{pd} = 2400$. and the other parameters used are $\boldsymbol{F}_B = 80,\ 200,\ 200,$ and 350, respectively, $\boldsymbol{F}_A$ is fixed at 200, $\Gamma = 2.5$, $\rho = 0.245$, $\omega_A = \omega_B = 0$.

In figure 4(*a–d*), typical simulation snapshots recorded for different values of external magnetic field strength ranging from $\beta = 0.001$ to $\beta = 1.0$ are shown. In the application of constant external non-parallel fields $\boldsymbol{F}_A$ and $\boldsymbol{F}_B$, the formation of tilted lanes are observed for all the values of β, which are in the direction of the force difference vector as expected. We have studied how the geometric structures of the lanes, i.e. the lane width and lane numbers, is affected by the magnetic field strength. It is seen that the thickness of the lanes involves several particle layers for $\beta = 0.001$, as can be seen in figure 4(*a*), and is comparable to the size of the simulation box. However, with increasing β value, it is noticed that the lane width decreases gradually (see figure 4*b–d*). The snapshots of states

https://doi.org/10.1017/S0022377823000387 Published online by Cambridge University Press

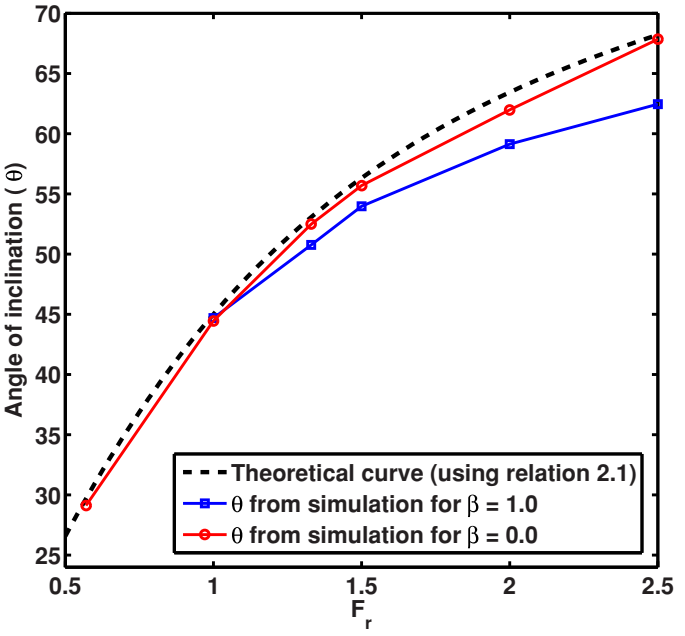

FIGURE 3. Angle of inclination (θ) versus electric field ratio (F_r) plot of the 3-D PIP system with non-parallel external fields taking $\boldsymbol{F}_r = \boldsymbol{F}_A/\boldsymbol{F}_B = 0.57$, 1.0, 2.0, 2.5, both in the absence ($\beta = 0$) and presence ($\beta = 1$) of the external magnetic field as obtained from LD simulation and using (2.1). The other parameters used are $\Gamma = 2.5$, $\rho = 0.245$. Here, the applied forces are constant in nature ($\omega_A = \omega_B = 0$).

in figure 4(*a–d*) also show that the number of lanes apparently depends on the β values, as the lane number gradually increases with increasing β. In contrast, with decreasing lane thickness, the order parameter (ϕ) measured along the direction of the difference vector is also found to be deceased with increasing β, as indicated in figure 4(*e*), where the order parameter (ϕ) is plotted against $t\omega_{pd}$ for $\beta = 0.001$, 0.01, 0.1 and 1.0, with $F_A = 200$ and $F_B = 100$.

In figure 5(*a*), the instantaneous particle snapshots of the x–z plane showing tilted lanes are plotted, both in the absence ($\beta = 0$) and presence ($\beta = 1.0$) of the external magnetic field. Here, positively charged PIP particles are drifting in the z-direction with external electric force $\boldsymbol{F}_A = 200$, while the negatively charged PIP particles are drifting in the x-direction with electric force $\boldsymbol{F}_B = 100$. The other parameters are $\Gamma = 2.5$, $\rho = 0.245$ and $\omega_A = \omega_B = 0$. Here, the angle of inclination (θ), i.e. the angle formed by the intersection of the tilted lane with the x-axis, is measured using the concept of analytic geometry. In analytic geometry, if the coordinates of three points A, B and C are known, then the angle between the lines AB and BC (see figure 5*a*) can be calculated as follows. From the snapshots in figure 5(*a*), it is observed that the tilted lanes are perfectly linear and for a line whose endpoints are $A(x_1, y_1)$ and $B(x_2, y_2)$, the slope of the line is given by the equation

$$m_1 = \frac{y_2 - y_1}{x_2 - x_1}. \tag{3.1}$$

The angle between the two lines AB and BC (see first column of figure 5*a*) can be found by calculating the slope of each line and then using them in (3.2) to determine the angle

https://doi.org/10.1017/S0022377823000387 Published online by Cambridge University Press

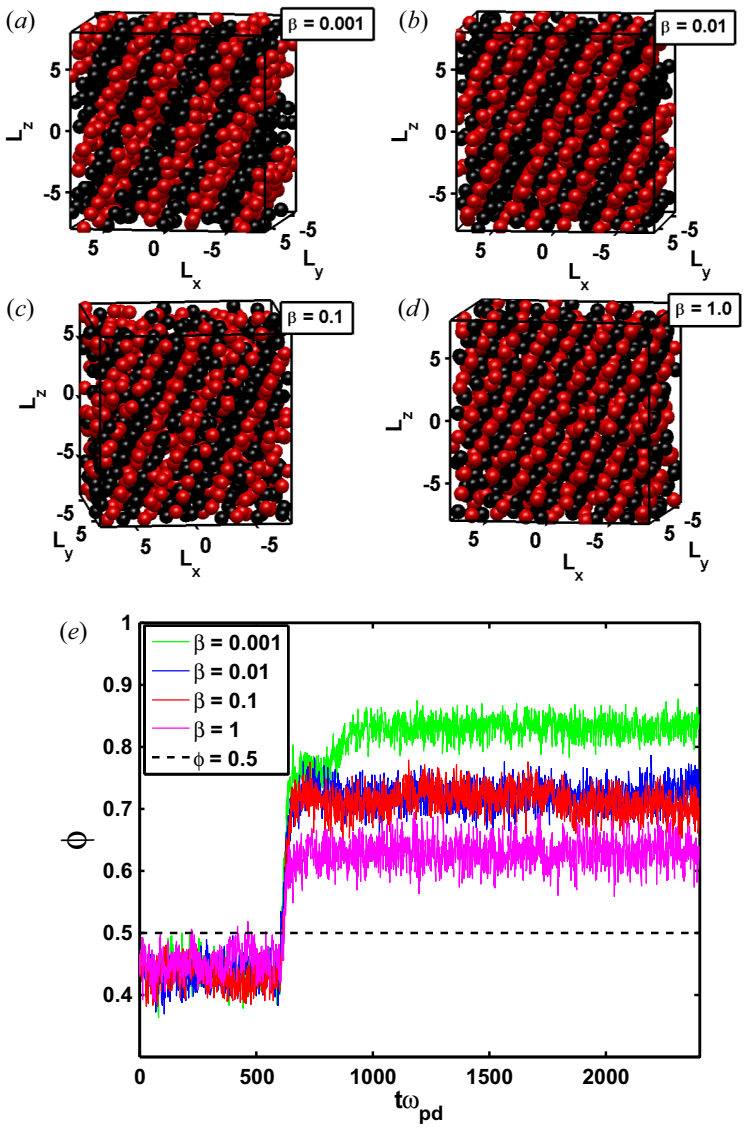

FIGURE 4. Typical simulation snapshots of the 3-D PIP system with perpendicular external fields. Here, $\boldsymbol{F}_A = 200$, $\omega_A = 0$, $\boldsymbol{F}_B = 100$, $\omega_B = 0$ are applied along the z- and x-directions. The snapshots are recorded for different values of the external magnetic field strength: (*a*) 3-D view with $\beta = 0.001$; (*b*) $\beta = 0.01$; (*c*) $\beta = 0.1$; (*d*) $\beta = 1.0$. (*e*) Time variation of order parameter (ϕ) plot corresponding to panels (*a–d*). The external magnetic field is applied in the y-direction. The other parameters used are $\Gamma = 2.5$, $\rho = 0.245$. The snapshot is recorded at the $t\omega_{pd} = 2400$ time step.

between two lines when the slope of each line is known from (3.1),

$$\left.\begin{aligned} \tan(\theta) &= \pm\frac{m_2 - m_1}{1 + m_1 m_2} \\ \Rightarrow \quad \theta &= \tan^{-1}\left(\frac{m_2 - m_1}{1 + m_1 m_2}\right) \end{aligned}\right\}. \tag{3.2}$$

https://doi.org/10.1017/S0022377823000387 Published online by Cambridge University Press

Using (3.2), the angle of inclination (θ) is measured in the absence of an external magnetic field with $\beta = 0$ (see figure 5*a*) as $\theta = 62.63^\circ$. Similarly, in the presence of an external magnetic field with $\beta = 1.0$, the angle of inclination is calculated as $\theta = 59.82^\circ$ (see figure 5*b*). However, the angle of inclination θ when measured in terms of the applied electric field strengths, it is found as $\theta = \tan^-(|\boldsymbol{F}_A|/|\boldsymbol{F}_B|) = \tan^{-1}(200/100) = 63.435^\circ$. In conclusion, this measured angle is quite consistent with the angle measured geometrically, which is approximately $\theta = 62.63^\circ$ with $\beta = 0$. However, for $\beta = 1.0$, $\theta = 59.82^\circ$, which further shows that the presence of a magnetic field influences the orientation of lanes (i.e. θ).

Figure 6(*a*) indicates the angle of inclination θ calculated using simulation data versus $t\omega_{pd}$ plot for a 3-D PIP system in the presence of non-parallel external electric fields taking different values of $\beta = 0.0$, 0.001, 0.01, 0.1 and 1. Comparing $\beta = 0$ with $\beta \neq 0$, it is observed that in the presence of a weak external magnetic field, the angle of inclination remains consistent with the $\beta = 0$ case; however, it is not observed in the presence of a strong magnetic field ($\beta = 1.0$). The magnitude of inclination ($|\theta|$) reduces for a higher β case. Further, it is also noted that depending on the direction of the external electric fields, the angle of inclination switches its domain due to the change in direction of the force difference vector. Initially, when $\boldsymbol{F}_A$ is applied along the positive z-direction and $\boldsymbol{F}_B$ is along the positive x-direction, the θ values are recorded as always positive as can be seen from figure 2. However, from figure 6(*a*), when $\boldsymbol{F}_A$ is applied along the positive z-direction and $\boldsymbol{F}_B$ is along the negative x-direction, the domain of θ is switched and θ is shown to be negative. However, $|\theta|$ remains the same for both cases. To account for the errors in measurement of θ plotted in figure 6(*a*), the distribution of $\Delta\theta$ is plotted for different values of $\beta = 0.0$, 0.001, 0.01, 0.1 and 1 in figure 6(*b*). Figure 6(*b*) helps in resolving the fluctuations observed in the time variation of the θ curve. It is observed that the distribution is almost Gaussian for all values of β. There is no significant change with small changes in β, i.e. for $\beta = 0.0$, 0.001, 0.01 and 0.1; however, a change in angle of inclination value and the distribution curve is noticed for $\beta = 1$.

3.2. *Time varying electric field*

In this sub-section, we report on the comprehensive simulation studies of lane formation in a 3-D PIP system that are carried out in the presence of perpendicular oscillatory external electric fields $\boldsymbol{F}_A$ and $\boldsymbol{F}_B$. Specifically, three different cases are discussed: *Case 1:* when $\boldsymbol{F}_A$ is oscillatory ($\omega_A \neq 0$) and $\boldsymbol{F}_B$ is constant ($\omega_B = 0$); *Case 2:* both $\boldsymbol{F}_A$, $\boldsymbol{F}_B$ are oscillatory having same frequencies ($\omega_A = \omega_B \neq 0$); *Case 3:* both $\boldsymbol{F}_A$, $\boldsymbol{F}_B$ are oscillatory having different frequencies ($\omega_A \neq \omega_B \neq 0$).

3.2.1. *Case 1: $\boldsymbol{F}_A$ is oscillatory ($\omega_A \neq 0$) and $\boldsymbol{F}_B$ is constant ($\omega_B = 0$)*

As observed in the constant electric field case, where two non-parallel constant ($\omega_A = \omega_B = 0$) external electric fields are applied perpendicular to each other, the lanes were formed in the direction of the difference vector (i.e. $\boldsymbol{F}_A - \boldsymbol{F}_B$) of the two external field vectors (see figure 2). The angle of inclination proved to be consistent with (2.1). Similar formation of a lane is observed in the presence of external time-varying and constant non-parallel forces. However, the orientation of the lanes does not remain fixed, it oscillates.

In figure 7(*a*), a series of simulation snapshots are shown for a 3-D PIP system in the presence of external fields where force $\boldsymbol{F}_A$ is time varying in nature with $\omega_A = 0.001$, applied along the z-direction, while $\boldsymbol{F}_B$ is applied along negative x-direction is a constant in nature with $\omega_A = 0.0$. Here, $\boldsymbol{F}_A$, $\boldsymbol{F}_B$ have field strengths $E_A = 200$, $E_B = 100$, respectively.

https://doi.org/10.1017/S0022377823000387 Published online by Cambridge University Press

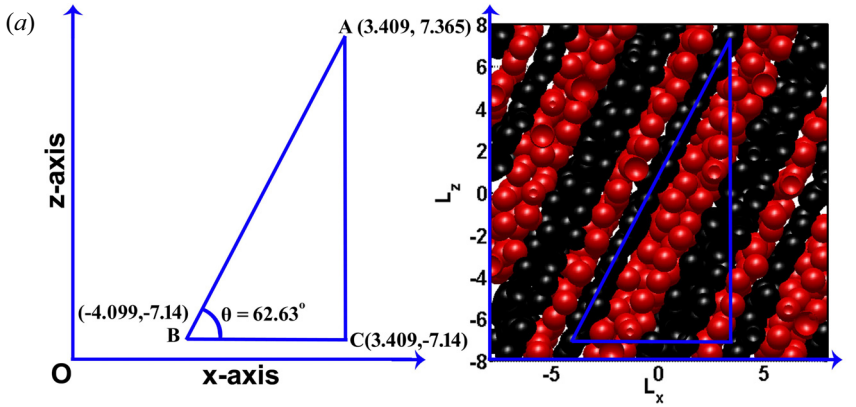

The instantaneous snapshot of X, Z plane.
Angle of inclination measured is $\theta = 62.63^0$ with $\beta = 0.0$

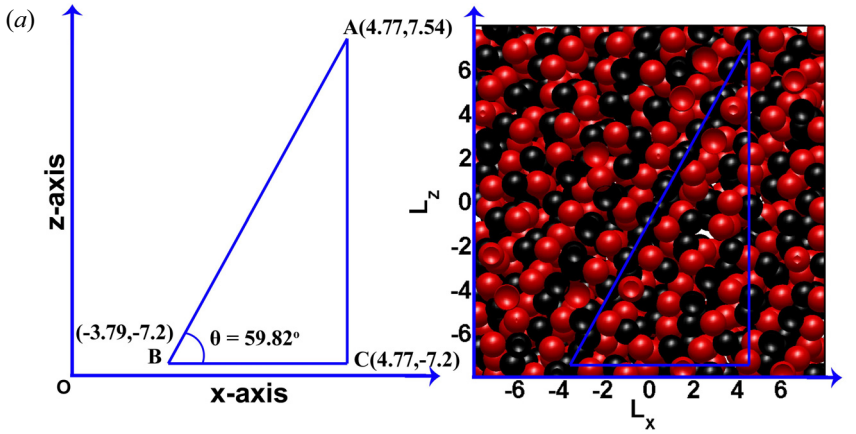

The instantaneous snapshot of X, Z plane.
Angle of inclination measured is $\theta = 59.82^0$ with $\beta = 1.0$

FIGURE 5. Instantaneous snapshot of the x–z plane, both in the (a) absence ($\beta = 0$) and (b) presence ($\beta = 1.0$) of the external magnetic field, of a 3-D PIP system with perpendicular external fields showing tilted lanes. The first column of the figure indicates the angle of inclination (θ) of the lanes with the x-axis. Here, half of the PIP particles are drifting in the z-direction with force $\boldsymbol{F}_A = 200$, while the other half of the PIP particles are drifting in the x-direction with force $\boldsymbol{F}_B = 100$. The external magnetic field is applied along the y-axis. The particles are rendered as spheres. For these snapshots, we simulate $N = 1000$ PIP particles. The parameters are $\Gamma = 2.5$, $\rho = 0.245$. The snapshot is recorded at the $t\omega_{pd} = 1620$ time step. In panel (a), the angle of inclination measured is $\theta = 62.63^\circ$ with $\beta = 0.0$. In panel (b), the angle of inclination measured is $\theta = 59.82^\circ$ with $\beta = 1.0$.

The instantaneous values of two electric field vectors $\boldsymbol{F}_A$ and $\boldsymbol{F}_B$ are represented by using two perpendicular arrows along the z- and x-axis, respectively (see figure 7a). The length of the vectors indicates the strength of the electric field and the direction of the arrow head indicates the direction of the electric field vector at any particular instant of time. From figure 7(a), it is realised that due to the oscillating nature of one of the external fields, the angle of inclination 'θ' between the formed lanes and x-axis is found to be time varying in nature which is dependent on the frequency of the applied field. The lanes tend to rotate in

https://doi.org/10.1017/S0022377823000387 Published online by Cambridge University Press

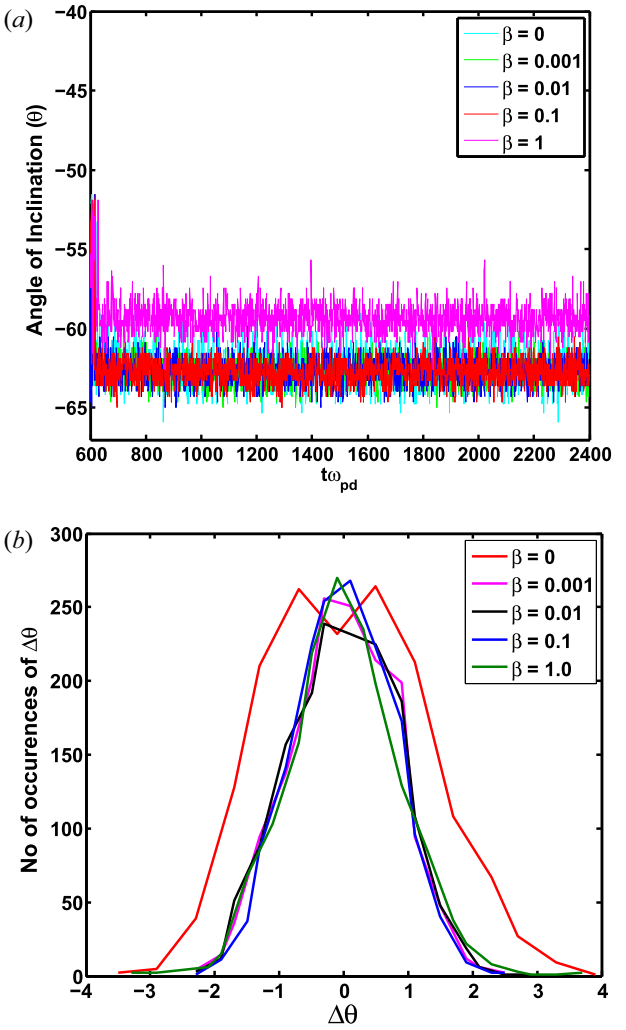

FIGURE 6. (*a*) Time variation of angle of inclination (θ) plot in the presence of an external magnetic field with strength values $\beta = 0.001, 0.01, 0.1, 1.0$, for a PIP system with non-parallel fields. (*b*) Distribution of $\Delta\theta$ (in degrees) for β values corresponding to panel (*a*). The parameters used are $\Gamma = 2.5$, $\rho = 0.245$ and $\omega_A = \omega_B = 0$. Here, $\boldsymbol{F}_A = 200$ is applied in the positive z-direction and $\boldsymbol{F}_B = 100$ is applied in the negative x-direction.

a counterclockwise direction. When inclination of lanes changes from one θ value to the other, a partial mixed state is observed, which may be caused due to the reorientation of the lanes. Additionally, as a consequence of the time-varying nature of one of the applied fields, the corresponding force $\boldsymbol{F}_A$ also varies with time (see figure 7*a*), which in turn changes the value of θ with time as observed from simulation (see figure 7*b*). Figure 7(*b*) indicates that the magnitude of the angle of inclination ($|\theta|$) becomes minimum when the field reaches its minimum value and when with time the field value reaches its maximum, the $|\theta|$ reaches a maximum too. The corresponding times when the instantaneous positions of particles are recorded is represented in figure 7(*a*). In figure 7(*a*), the initial snapshot at $t\omega_{pd} = 648$ is taken just after some time of application of the external fields at the $t\omega_{pd} = 600$ time step, and the corresponding θ from simulation is recorded as -58.40°.

https://doi.org/10.1017/S0022377823000387 Published online by Cambridge University Press

The next snapshot is taken at $t\omega_{pd} = 1188$, with θ increased to -37.95°. Further, in the snapshot recorded at $t\omega_{pd} = 1512$, the θ is increased to -11.56°. From the next snapshots recorded at $t\omega_{pd} = 1671, 1998, 2400$, it is observed that the electric field vector $\boldsymbol{F}_A$ changes its direction and is pointing towards the negative z-direction, and the corresponding values of angle of inclination are found from the simulation as $\theta = 9.89^\circ, 37.06^\circ, 55.66^\circ$, respectively. Further, the angle of inclination θ is also calculated using (2.1). By randomly considering any two simulation snapshots at times $t\omega_{pd} = 648$ and 1998, the calculated θ (using (2.1)) is recorded as $\theta = -57.89^\circ, 39.65^\circ$, respectively, which are very close to the practically obtained values (from simulation) of $\theta = -58.40^\circ, 39.06^\circ$, respectively, recorded for the above mentioned simulation times. Similarly, upon calculating θ for all the simulation snapshots plotted in figure 7(*a*), it is observed that in the absence of an external magnetic field (i.e. $\beta = 0$), the calculated value of θ using (2.1) is in close agreement with data obtained directly from simulation.

Further, to understand the effect of the electric field strength and frequency on the variation of angle of inclination θ, in figure 8, θ is plotted versus $t\omega_{pd}$ for different values of the ratio between amplitudes of the non-parallel electric fields $E_A/E_B = 0.57$, 1.0, 2.0 and 2.5, which is obtained by varying E_B as 350, 200, 100 and 80, respectively, keeping the E_A value fixed at 200. The electric field applied along the z-direction is considered as time varying ($\omega_A = 0.001$) in nature; however, the electric field applied along the x-direction is constant ($\omega_A = 0$) in nature. The other parameters used are $\Gamma = 2.5$, $\rho = 0.24$ and $\beta = 0$. Figure 8 indicates variation of θ with time, ranges from $+\theta$ to $-\theta$ for all values of E_A/E_B; however, this range of θ variation gradually increases with increasing E_A/E_B value. The range of θ variation is also calculated using (2.1). For $E_A/E_B = 2.5$, the θ range is calculated using (2.1) as $[-68.2^\circ, +68.0^\circ]$, and for $E_A/E_B = 0.57$, it is found as $[-29.74^\circ, +29.74^\circ]$. However, for $E_A/E_B = 2.0$, 1.0, the θ value range is found as lying in between the $E_A/E_B = 2.5$ and 0.57 cases. Further, it is also noticed that for all values of E_A/E_B, the range of θ variation obtained directly from simulation is consistent with the calculated one in the absence of an external magnetic field and this can be better visualised from figure 9. In figure 9(*a*), the angle of inclination is plotted versus $t\omega_{pd}$ in the presence of non-parallel forces $\boldsymbol{F}_A$ and $\boldsymbol{F}_B$; $\boldsymbol{F}_A$ is of oscillatory type and $\boldsymbol{F}_B$ is of constant one. The amplitude of the electric field associated with $\boldsymbol{F}_A$ is considered as $E_A = 200$, having field frequencies $\omega_A = 0.001, 0.01$; for force $\boldsymbol{F}_B$, the field strength is chosen as $E_B = 350$, with field frequency $\omega_B = 0$, so that E_A/E_B becomes 0.57. In figure 9(*a*), we plot the results of our calculation done by using (2.1) for the same parameter combinations as chosen for the simulations in figure 8; however, results for all data sets are not included. Comparing calculated and simulation results, the calculation reproduces all trends correctly. In particular, θ variation range grows with increasing E_A/E_B (results for all E_A/E_B values are not mentioned here), and are not affected by different values of the applied field frequencies (here, results for frequency values $\omega_A = 0.001, 0.01$ are only shown), as obtained in the simulations. As shown in figure 9(*a*), for $E_A/E_B = 0.57$, the θ variation range is observed as [-30°, 30°], as indicated by pink and yellow dashed lines; and exactly the same range of θ variation is observed for both $\omega_A = 0.001$ (see figure 9*a*,*b*) and $\omega_A = 0.01$ (see figure 9*a*) values. Furthermore, from figure 9, it is also noticed that with increasing the field frequency value (ω_A) of the oscillatory force $\boldsymbol{F}_A$, the frequency of oscillation of θ, i.e. ω_θ, also increases.

Simulation snapshots of a situation with non-parallel forces having $E_A = 200$, $\omega_A = 0.001$ applied along the z-direction and $E_B = 350$, $\omega_B = 0$ applied along the x-direction are shown in figure 10. One clearly sees random oscillations of the PIP system between ordered lane state and a disordered mixed state with its own characteristic frequency (say, ω_{break}, where lanes break). In figure 10, the first snapshot is taken at $t\omega_{pd} = 737$

https://doi.org/10.1017/S0022377823000387 Published online by Cambridge University Press

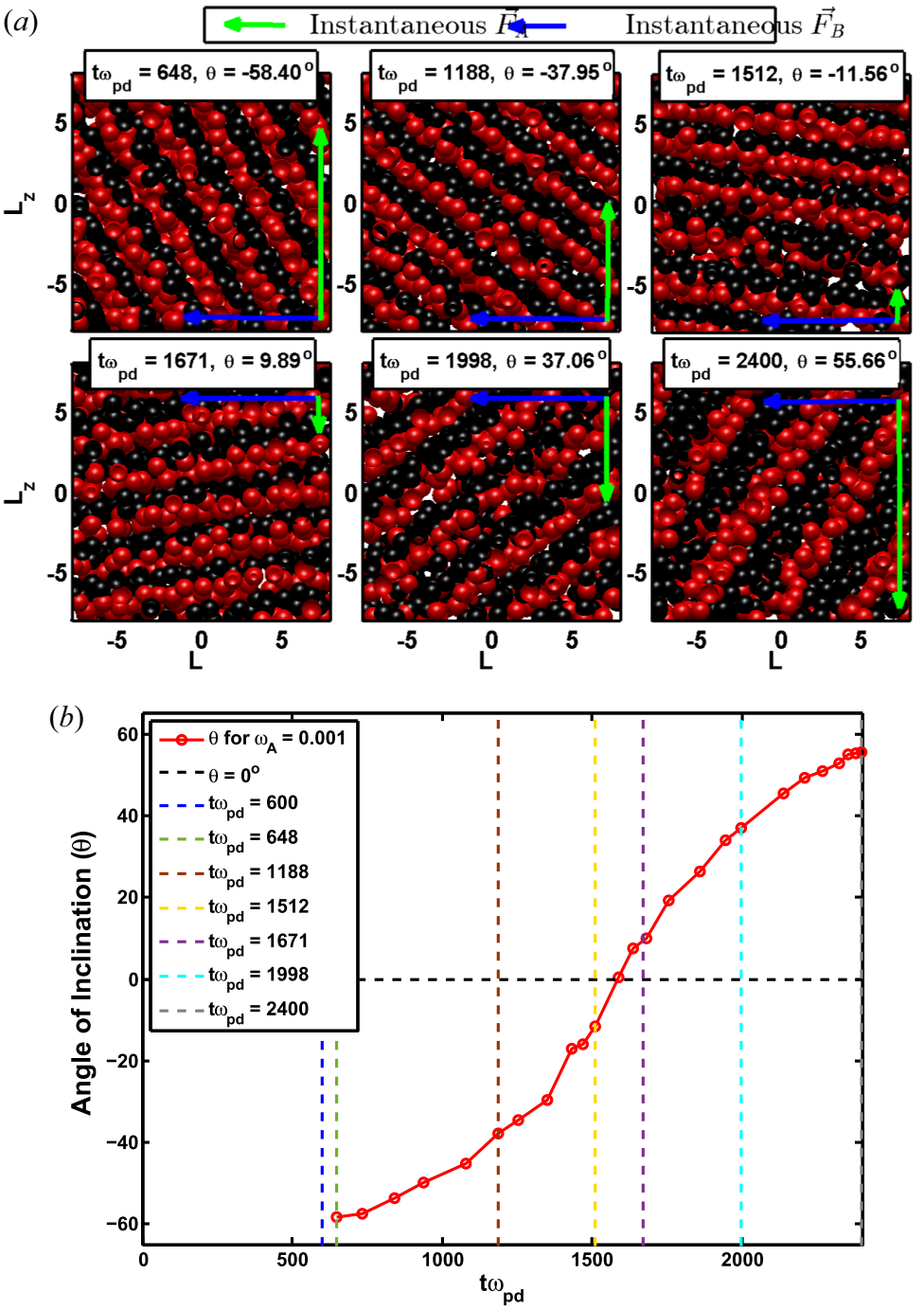

FIGURE 7. (*a*) Typical simulation snapshots of the 3-D PIP system. The snapshots are recorded at the $t\omega_{pd} = 648$, 1188, 1512, 1671, 1998 and 2400 simulation time steps. (*b*) Angle of inclination 'θ' (in degree) variation plot versus $t\omega_{pd}$ of the 3-D PIP system, plotted during simulation. The corresponding times, denoted by different coloured dashed lines, when the instantaneous positions of particles are recorded is represented in panel (*a*). Here, the external electric force $\boldsymbol{F}_A$ is applied along the z-direction having field strength $E_A = 200$, frequency $\omega_A = 0.001$ and $\boldsymbol{F}_B$ is applied along the x-direction of field strength $E_B = 100$, frequency $\omega_B = 0$. The other parameters used are $\Gamma = 2.5$, $\rho = 0.24$.

https://doi.org/10.1017/S0022377823000387 Published online by Cambridge University Press

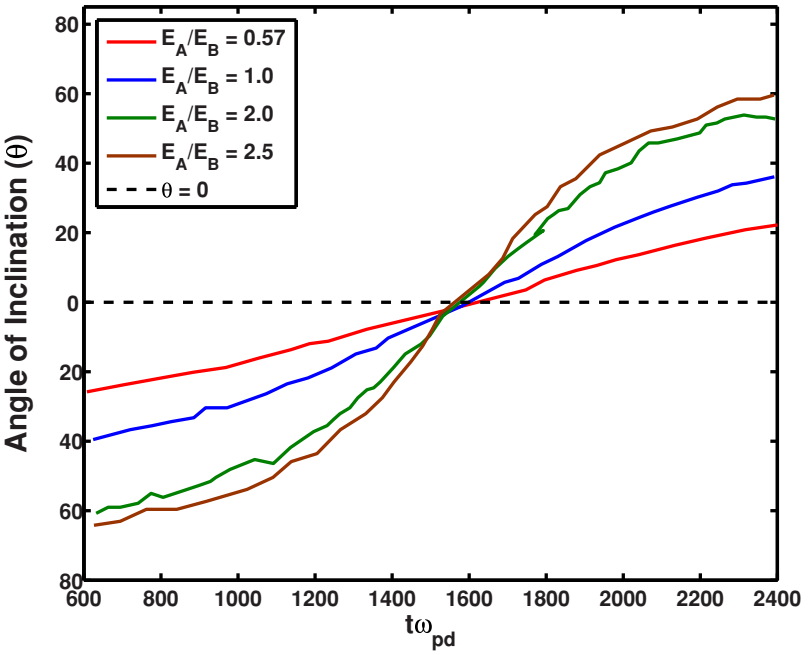

FIGURE 8. Comparative angle of inclination 'θ' (in degree) variation versus $t\omega_{pd}$ plot of the 3-D PIP system for different values of the ratio between amplitudes of the non-parallel electric fields $E_A/E_B = 0.57$, 1.0, 2.0, 2.5. The other parameters used are $\Gamma = 2.5$, $\rho = 0.24$ and $\beta = 0$. The external electric force $\boldsymbol{F}_A$ is applied along the z-direction having field strength $E_A = 200$, frequency $\omega_A = 0.001$ and $\boldsymbol{F}_B$ is applied along the x-direction of field strength $E_B = 350$, 200, 100, 80, having frequency $\omega_B = 0$.

where ordered lanes are clearly visible with an angle of inclination $\theta = -23.3^\circ$ made with the x-axis. The order parameter, when measured in a direction parallel to the lanes, $\phi(\theta)$, is found to be 0.6144. In the next snapshot taken at $t\omega_{pd} = 780$, the ordered lane is broken and a mixed phase is obtained with $\phi(\theta) = 0.4377$. The snapshot taken at $t\omega_{pd} = 807$ identifies the lane state again with $\phi(\theta) = 0.8012$ and the corresponding angle of inclination is recorded as $\theta = -21.7^\circ$, which is slightly greater than that obtained for the first snapshot. This is then followed by a disordered state again with $\phi(\theta) = 0.4112$. The last two snapshots are taken at $t\omega_{pd} = 965$ and 1020, with $\phi(\theta) = 0.8393$ and 0.4431, respectively. The value of the angle of inclination recorded at $t\omega_{pd} = 965$ is $\theta = -18.5^\circ$. The corresponding angle of inclination (θ) versus $t\omega_{pd}$ plot is shown in figure 11. Figure 11(b) is the zoomed plot from $t\omega_{pd} = 700$ to $t\omega_{pd} = 1055$ where the instantaneous position of the particles are recorded. Here the black lines represent the regions when the system reaches the mixed-ordered phase. We remark that between consecutive θ values, lanes may fuse towards small non-structured regions.

To better visualise the embedded frequency of the breaking and formation of lanes or frequency of reorientation, i.e. ω_{break}, corresponding to the set of runs mentioned in figure 11, the order parameter with gradient of θ ($\phi(\theta)$) versus $t\omega_{pd}$ is plotted in figure 12(a), where, a gradient of θ exists along the x-axis. The colour bar represents the direction θ (in degrees) at which the measurement is taken. It is noticed that the system repeatedly transits from a lane state to a no lane state with a characteristic frequency of $\omega_{\text{break}} = 0.07$. This characteristic frequency is determined using fast Fourier

https://doi.org/10.1017/S0022377823000387 Published online by Cambridge University Press

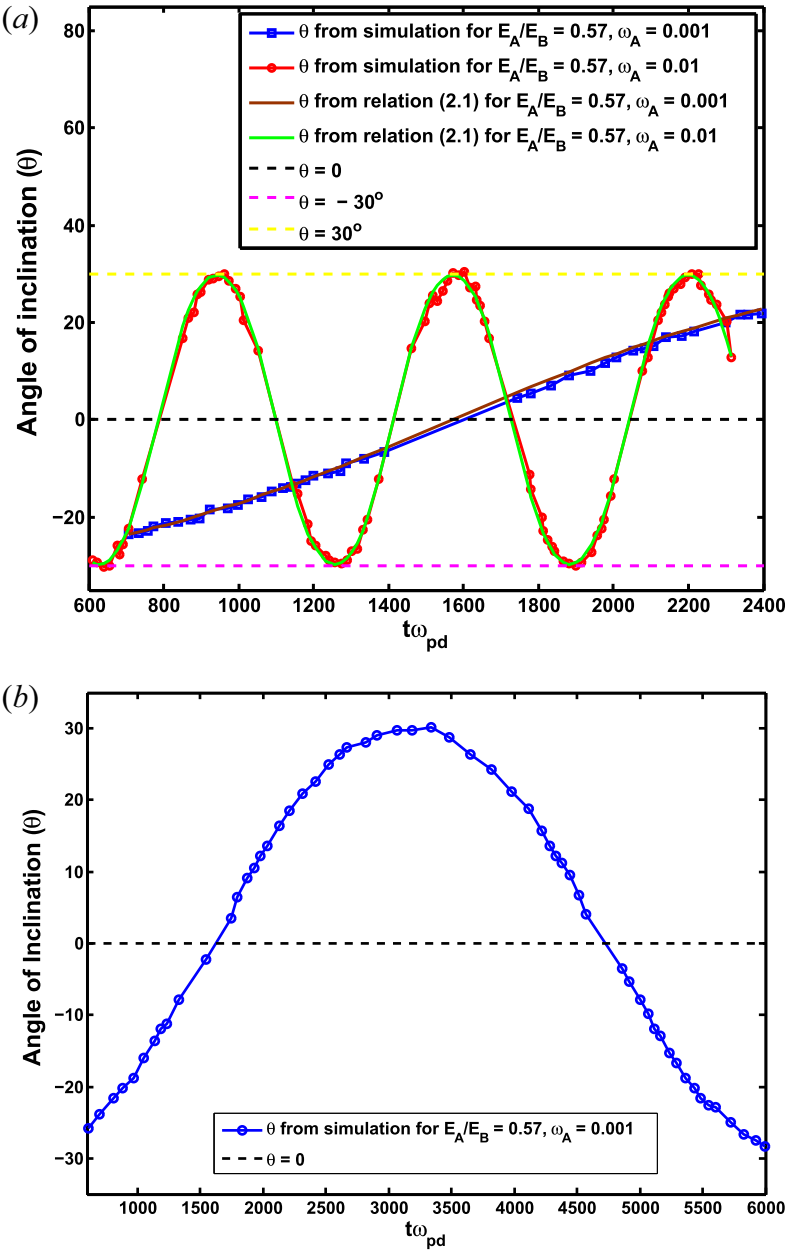

FIGURE 9. (*a*) Angle of inclination 'θ' (in degree) variation with $t\omega_{pd}$ of the 3-D PIP system showing simulation data along with the theoretical curve in the presence of an oscillatory external electric field having field strength $E_A = 200$, frequency values $\omega_A = 0.001$ and 0.01. (*b*) Angle of inclination 'θ' variation with $t\omega_{pd}$ for a long simulation time of $t\omega_{pd} = 6000$ taking $E_A = 200$, $\omega_A = 0.001$. Here, the other field is applied having field strength $E_B = 350$ and $\omega_B = 0$. The whole study is performed in the absence of a magnetic field ($\beta = 0$). The other parameters used are $\Gamma = 2.5$, $\rho = 0.24$.

https://doi.org/10.1017/S0022377823000387 Published online by Cambridge University Press

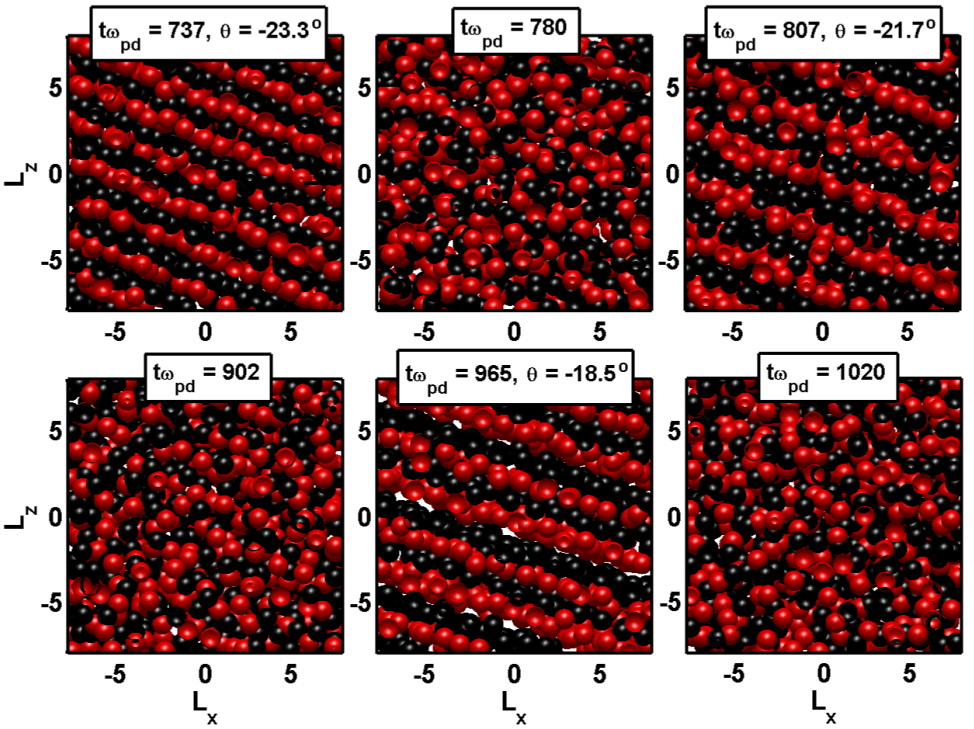

FIGURE 10. Typical simulation snapshots of the 3-D PIP system with oscillatory external electric field having frequency values $\omega_A = 0.001$ and $\omega_B = 0.0$, and field strength $E_A = 200$ and $E_B = 350$ is constant in nature. The snapshots are recorded at time $t\omega_{pd} = 737$, 780, 807, 902, 965 and 1020. The other parameters used are $\Gamma = 2.5$, $\rho = 0.24$ and $\beta = 0$.

transformation shown in figure 12(*b*). Here, a significant peak at 0.07 indicates the frequency at which $\phi(\theta)$ oscillates. Another significant peak is obtained at 0.001 which accounts for the applied frequency of the external force. Further, this is also evident from the order parameter value: $\phi(\theta) \geq 0.5$ indicates a lane state and $\phi(\theta) < 0.5$ indicating a no lane state. The related snapshots taken at different simulation times plotted in figure 10 are also consistent with our observation. It is also noticed that the frequency of the formation and breaking of lanes is not equal to the frequency of the applied external field, i.e. $\omega_{\text{break}} \neq \omega_A$, which may lead to the assumption that this behaviour is exhibited due to a reorientation of the angle of inclination θ where the system generates the frequency ω_{break}. Whenever θ is changed from one value to another, the electric field forces the lanes to reorient themselves in the direction parallel to the difference vector of the two externally applied electric fields. This breaks the lane structure and forms new lanes in a new direction parallel to the changed difference vector. Another diagnostic technique is implemented to test the stability of the lanes where the time duration of each lane state or no lane state is calculated. The counter basically measures the time duration for which the system remains in the lane state. This time duration is plotted along the x-axis in figure 12(*c*). Subsequently, another counter measures the time duration for which the system remains in the no lane or disordered state. This time duration is plotted along the x-axis of figure 12(*d*). There are various instances in the same run when the system is in the lane state. The number of occurrences given on the y-axis indicates these instances. In other words, the two counters calculate the width of every spike and dip in $\phi(\theta)$ in a

https://doi.org/10.1017/S0022377823000387 Published online by Cambridge University Press

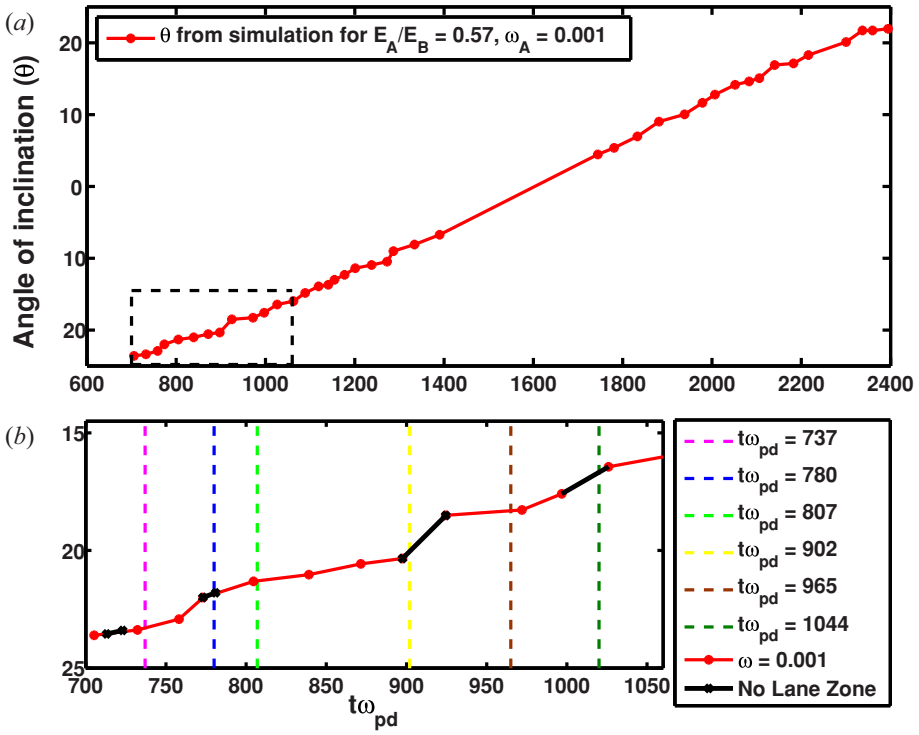

FIGURE 11. (*a*) Angle of inclination 'θ' (in degree) variation with $t\omega_{pd}$ of the 3-D PIP system. The external electric force $\boldsymbol{F}_A$ is applied along the z-direction having field strength $E_A = 200$, frequency $\omega_A = 0.001$ and $\boldsymbol{F}_B$ is applied along the x-direction having field strength $E_B = 350$, frequency $\omega_B = 0$. The other parameters used are $\Gamma = 2.5$, $\rho = 0.24$ and $\beta = 0$. (*b*) Zoomed view of the bounded region indicating by black colour dash line in panel (*a*).

normalised time unit. The distribution of this time duration is then plotted. In figure 12(*c*), the distribution of the lane state time duration is shown for the same parameters used in figure 12(*a*). The peak at a time duration of 5 having a magnitude of 5 in figure 12(*a*) indicates that there are 5 instances when the system was in a lane state for 5 units of time. It is also observed that the time duration of the system being in the lane state is distributed within a wide range, however, most of the peaks are concentrated below $100\omega_{pd}$, indicating that most of the time, the system is in a lane state for less than $100\omega_{pd}$ units of time. Similarly, in figure 12(*d*), the distribution of the no lane state time duration is also shown. It is noted that similar to the lane state time duration plot, the peaks are distributed in a wide range and most of the peaks are concentrated below $150\omega_{pd}$. Considering the distribution in figure 12(*c*,*d*), it is concluded that the system transits rapidly from a lane state to no lane state and the lanes formed could be considered to be slightly unstable.

To determine the frequency of the oscillation of θ (ω_θ), the fast Fourier transformation technique is used. The angle of the inclination curve which is a function of time is decomposed into a function depending on the frequency using a Fourier transform. In figure 13, the θ versus $t\omega_{pd}$ plot is shown for two cases: $\boldsymbol{F}_A$ is applied having strength $E_A = 200$, frequencies (*a*) $\omega_A = 0.001$ and (*b*) $\omega_A = 0.01$; however, $\boldsymbol{F}_B$ is applied having strength $E_B = 350$, $\omega_B = 0.0$, for both cases. The other parameters used are $\Gamma = 2.5$, $\rho = 0.24$. The respective single-sided Fourier transformations of figure 13(*a*,*b*) are shown in figure 13(*c*,*d*), respectively. Significant appearance of peaks are observed in both the

https://doi.org/10.1017/S0022377823000387 Published online by Cambridge University Press

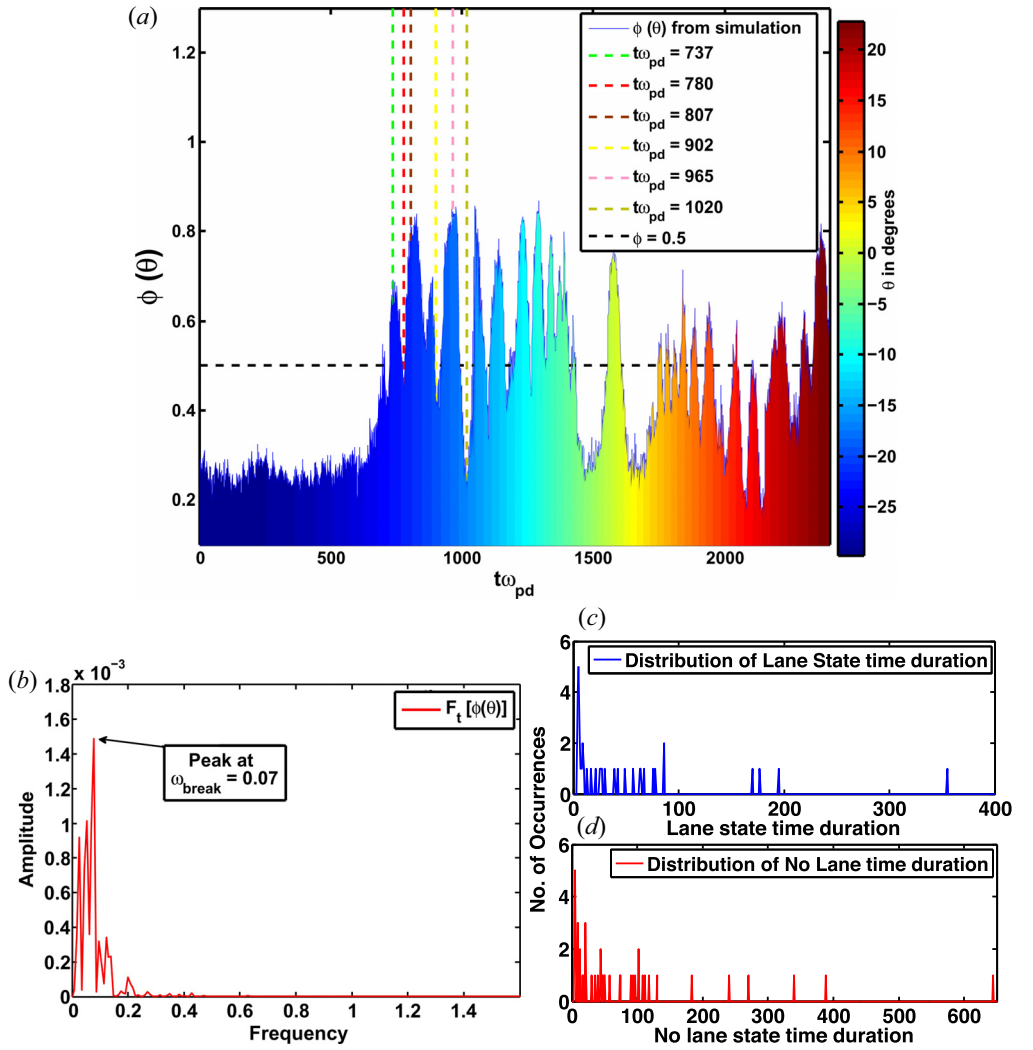

FIGURE 12. Order parameter with gradient of θ ($\phi(\theta)$) against $t\omega_{pd}$ in the presence of an oscillatory external electric field having frequency values $\omega_A = 0.001$ and $\omega_B = 0.0$ with field strength $E_A = 200$ and $E_B = 350$. The other parameters used are $\Gamma = 2.5$, $\rho = 0.24$. The colour bar indicates the angle of inclination in degrees for any instant of time. (*b*) Single-sided Fourier transform of function $\phi(\theta)$ is shown in panel (*a*). (*c*) Distribution of lane state time duration. (*d*) Distribution of no lane state time duration for the same parameters.

plots, which indicate that the frequency of oscillation of the quantity θ comes out to be $\omega_\theta = 0.0018$ for $\omega_A = 0.001$, and $\omega_\theta = 0.0107$ when $\omega_A = 0.01$. The obtained observation indicates that the frequency of oscillation of θ (i.e. ω_θ) and frequency of the applied external oscillatory force component (ω_A) are almost equal. Further, from the above results, it is also clear that θ oscillates back and forth between a range of fixed values. When it reaches a certain small value of θ close to -5° to $+5^\circ$, a partially formed lane structure parallel to the z-axis along with a partial mixed state are observed to coexist simultaneously, as indicated in figure 13(*e*,*f*) recorded at the $t\omega_{pd} = 1467$, 1119 simulation time steps, respectively.

https://doi.org/10.1017/S0022377823000387 Published online by Cambridge University Press

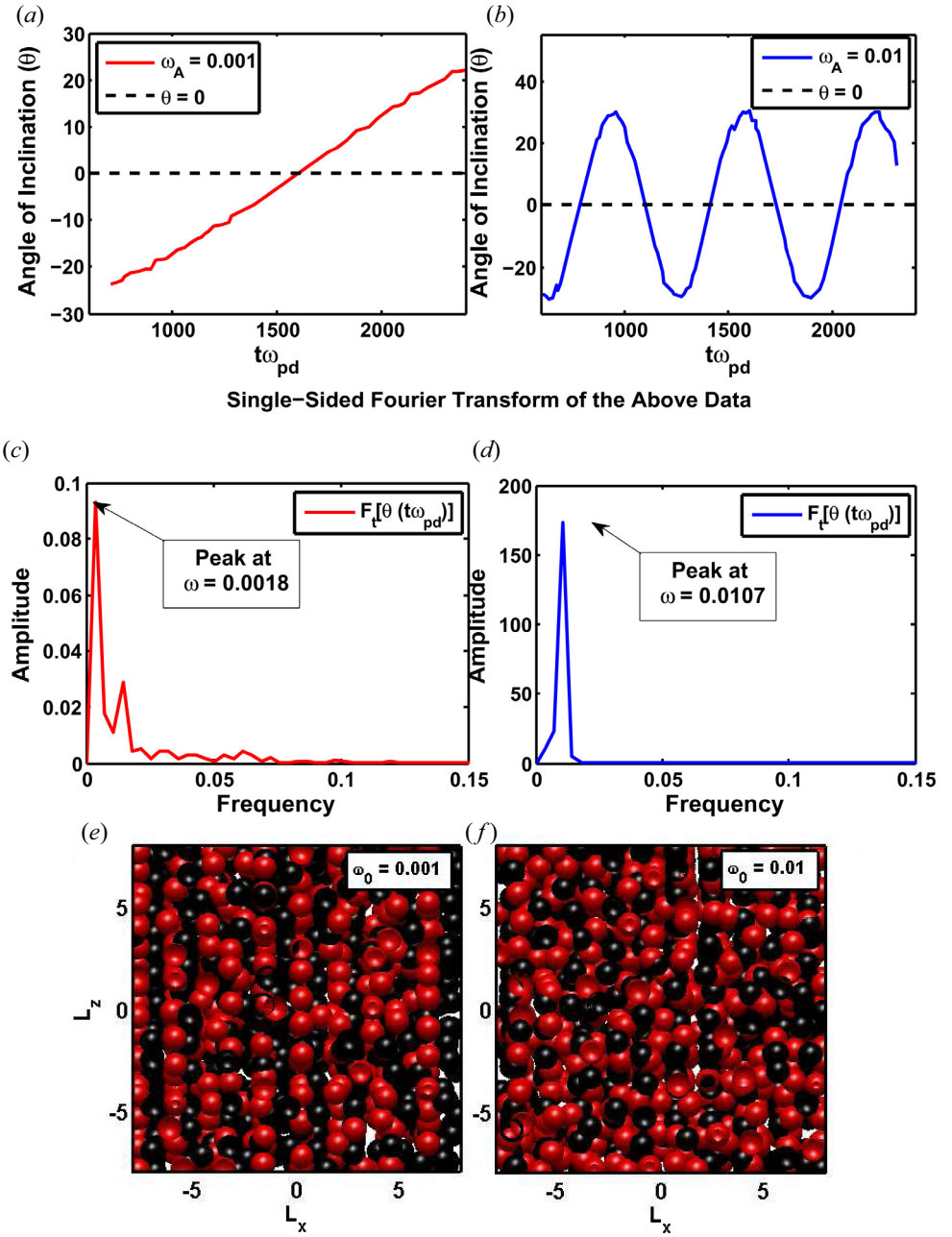

FIGURE 13. Angle of inclination 'θ' (in degree) plot of the 3-D PIP system in the presence of external electric fields with field strength $E_A = 200$ and frequency values (*a*) $\omega_A = 0.001$, (*b*) $\omega_B = 0.01$; the electric field applied perpendicular to E_A is $E_B = 350$, $\omega_B = 0$. The other parameters used are $\Gamma = 2.5$, $\rho = 0.24$. (*c*) Single-sided Fourier transform of curve in panel (*a*). (*d*) Single-sided Fourier transform of curve in panel (*b*). Simulation snapshots recorded at (*e*) $t\omega_{pd} = 1467$ and (*f*) $t\omega_{pd} = 1119$ related to panels (*a*) and (*b*), respectively.

https://doi.org/10.1017/S0022377823000387 Published online by Cambridge University Press

In the presence of a magnetic field ($\beta \neq 0$), half of the PIP particles are found to drift in the z-direction with force $\boldsymbol{F}_A$ which is time varying in nature, while the other half of the PIP particles are found to drift in the negative x-direction with force $\boldsymbol{F}_B$. Lanes are found to form when electric fields having a field strength greater than the critical electric field are applied to the system, similar to the case when a magnetic field is absent. The lanes formed are inclined in a direction parallel to the direction of the difference vector of the two externally applied forces. Like the previous case in the absence of a magnetic field, in the presence of a magnetic field, oscillation of θ with time is also observed. This oscillation of θ with time might be due to the fact that the presence of an oscillating force component results in the oscillation of the difference vector, which in turn tends to oscillate the angle of inclination of lanes formed with the x-axis. Varying the frequency of the applied oscillating force component (ω_A), the frequency of oscillation of θ (ω_θ) also varies accordingly, where $\omega_A \cong \omega_\theta$. Similar to the case when an external magnetic field is not present, the lanes have a tendency to break and re-form again, which could be induced by the reorientation of the lanes. The frequency of this spontaneous formation and breaking of lanes, i.e. ω_{break}, is found to be similar to that observed in the absence of an external magnetic field for the same set of parameters under study.

Figure 14 shows the angle of inclination versus $t\omega_{pd}$ plot by taking $E_A = 200$, $\omega_A = 0.001$, 0.01, and $E_B = 350$, $\omega_B = 0.0$ both in the presence ($\beta = 1.0$) and absence ($\beta = 0.0$) of a magnetic field. In the presence of a magnetic field, the range of θ values in the figure is found to be $[-32^\circ, +27^\circ]$ for $\omega_A = 0.01$ and $[-26^\circ, +17^\circ]$ for $\omega_A = 0.001$. It is observed that the presence of a magnetic field has shifted the curve or the range of θ values by almost -4° for $\omega_A = 0.001$ and -2° for $\omega_A = 0.01$ as compared to the range obtained in absence of the magnetic field; as mentioned below, with $\beta = 1.0$, the curve is shifted vertically downwards. This vertical shift is more for $\omega_A = 0.001$ than that of $\omega_A = 0.01$. This shift may be caused due to the force $\boldsymbol{F}_{\text{mag}} = Q_{A,B}(v \times \boldsymbol{B})$ exerted on the particles in the presence of magnetic fields. This indicates that (2.1) holds true if a magnetic field is absent. However, by modifying (2.1) and incorporating the effect of the external magnetic field (which is not done here), it might be possible to generate theoretically the θ versus $t\omega_{pd}$ plot of our system in the presence of an external magnetic field.

3.2.2. *Case 2:* $\omega_A = \omega_B \neq 0$

In the presence of non-parallel forces $\boldsymbol{F}_A$ and $\boldsymbol{F}_B$, where both force components are oscillatory in nature and have same frequency of oscillation $\omega_A = \omega_B = 0.001$, the angle of inclination no longer oscillates and becomes almost constant with $\omega_\theta \cong 0$. The system behaves in a similar way to the case when the force components are non-parallel and constant in nature with $\omega_A = \omega_B = 0$; however, some exceptions are observed as discussed later in the section. It could be due to the fact that the applied non-parallel external forces are interacting among themselves by the virtue of superposition leading to a resultant vector that has a constant direction but varying magnitude. Particles under the influence of perpendicular oscillatory fields follow a straight line path when the two fields are in phase. The slope of this resultant difference vector is given by the ratio of the amplitude of the applied fields, i.e. E_A/E_B which is a constant. In such cases, the oscillations are confined within one plane and the oscillations are said to be plane polarised. Therefore, a constant angle of inclination is observed when $\omega_A = \omega_B$; also, the lanes of particles form planes due to polarised oscillation which can be seen in the majority of snapshots shown above. In figure 15, instantaneous order parameter ϕ measured along the difference vector plotted versus $t\omega_{pd}$ are shown along with the time variation of the angle of inclination θ values. It is observed that the angle of inclination θ remains almost constant around $\theta = 29^\circ$ throughout the observed time domain, which is consistent with (2.1). However, initially,

https://doi.org/10.1017/S0022377823000387 Published online by Cambridge University Press

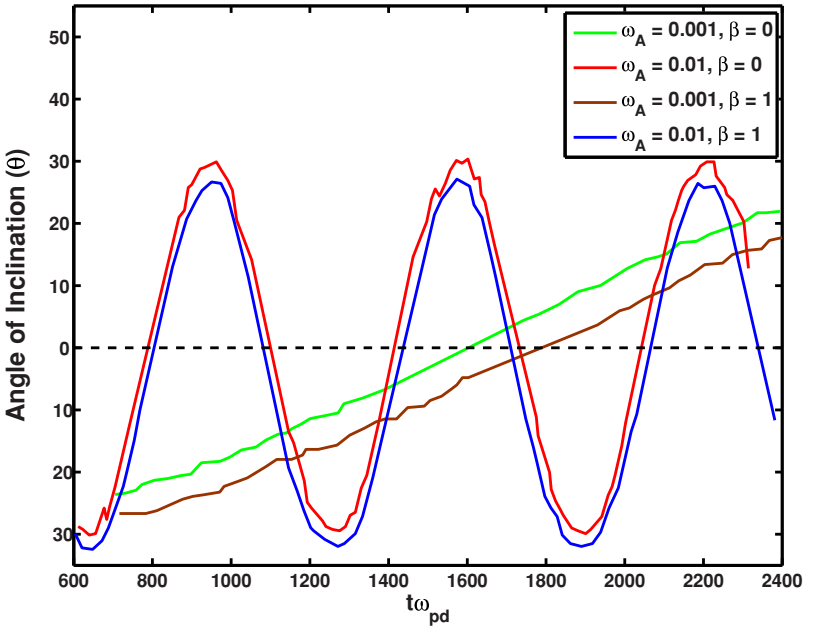

FIGURE 14. Comparative angle of inclination 'θ' (in degree) variation with $t\omega_{pd}$ of the 3-D PIP system in the presence of an oscillatory external electric field having frequency values $\omega_A = 0.001$ and 0.01 and field strengths $E_A = 200$ and $E_B = 350$ with frequency $\omega_B = 0.0$, in the presence ($\beta = 1$) and absence ($\beta = 0$) of a magnetic field. The other parameters used are $\Gamma = 2.5$, $\rho = 0.24$.

the order parameter plot indicates a highly self-organised state followed by a disordered state with $\phi = 0.372$ at $t\omega_{pd} = 1572$. As time passes, the system spontaneously regains the lane state as indicated by $\phi > 0.5$. In the figure, this disordered state is represented by a black line on the angle of inclination curve, as the no lane state occurs, therefore, no angle of inclination is measured in this region. The corresponding value of the frequency of order parameter oscillation is calculated as 0.0009 (here, 0.001 is the frequency of the applied fields). It is therefore concluded that the order parameter also oscillates with a frequency equal to the frequency of the applied external fields.

The time variation of the angle of inclination is shown in figure 16 for different values of $E_A/E_B = 2.5$, 2.1, 1.0 and 0.57, in the presence of non-parallel forces, force F_A having field strength $E_A = 200$, frequency $\omega_A = 0.001$ drifting along z-direction, while along the x-direction, force F_B is applied with variable field strengths $E_B = 80$, 100, 200 and 350, having the same frequency value $\omega_B = 0.001$ as that of ω_A. It is observed from the figure that θ remains constant throughout the time domain and $|\theta|$ decreases with decreasing E_A/E_B. Here, the negative sign of θ indicates that the direction of the difference vector is switched to the negative domain, this is due to the application of $\boldsymbol{F}_B$ along the negative x-direction of the simulation chamber. The no lane state is indicated by a black coloured line in the figure and it is appearing for almost a similar time duration and at the same time zone for the different values of E_A/E_B under study. Furthermore, the no lane state slowly disappears as the frequency of the applied external field increases gradually, which can be understood from figure 17(a), where the instantaneous order parameter ϕ is plotted for different values of frequencies $\omega_A = \omega_B = 0.001$, 0.01 and 0.1, for the same set of plasma parameters as mentioned above. It is evident from the figure that with increasing

https://doi.org/10.1017/S0022377823000387 Published online by Cambridge University Press

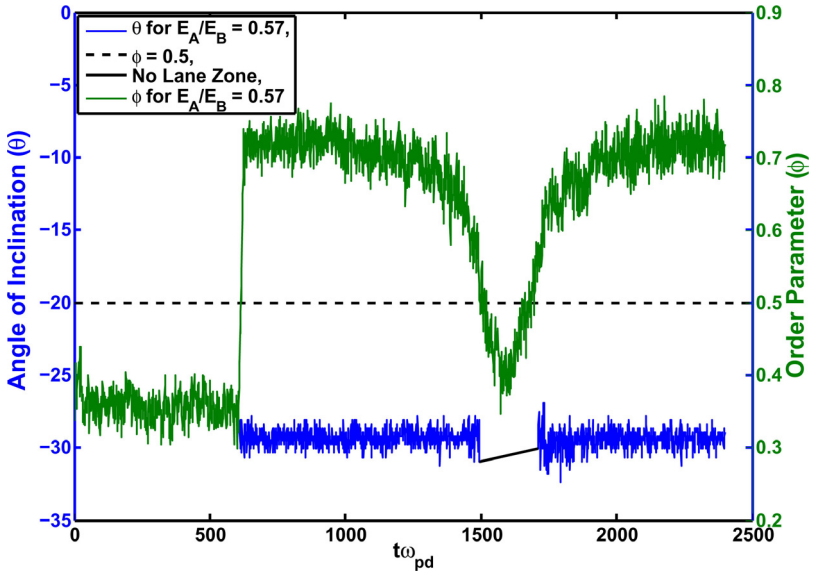

FIGURE 15. Comparative angle of inclination 'θ' (in degree) and order parameter ϕ variation with $t\omega_{pd}$ of the 3-D PIP system in the presence of non-parallel oscillatory external electric fields with field strength $E_A = 200$ and $E_B = 350$, with the same value of field frequency $\omega_A = \omega_B = 0.001$, in the absence ($\beta = 0$) of a magnetic field. The other parameters used are $\Gamma = 2.5$, $\rho = 0.24$. The black lines are not part of the data. They are drawn later to indicate the region when there is no lane state, as the lanes oscillate between the ordered and disordered state. When the system is in the lane state, the orientation of the lanes could be measured giving a real value for θ; however, when the system is in the no lane state, there is no question of measuring the angle of inclination. The angle of inclination is measured only when $\phi \geq 0.5$. The gap indicated by a black line is to highlight the fact that the measurement is not done as the system is in the no lane state.

frequency, the dip in the order parameter curve decreases slowly. This, in turn, decreases the time zone of the no lane state which disappears when $\omega_A = \omega_B = 0.1$ is approached. Increasing the frequency tends to reduce the tendency of spontaneous breaking of lanes when non-parallel oscillatory forces are applied to the system. A Fourier transformation is performed on $\phi(t\omega_{pd})$ to determine the frequencies associated with oscillation in ϕ. In figure 17(b), the Fourier transform is shown for $\omega_A = \omega_B = 0.001$, 0.01 and 0.1. It is observed that no peaks are obtained at the driving frequencies; however, one significant peak is obtained for all three cases at 0.003, 0.0201 and 0.1993 which is $\approx$3, 2 and 2 times the driving frequency, respectively. The system may be generating the observed frequency in response to the applied time-varying forces. It is also noted that for $\omega_A = \omega_B = 0.01$, several peaks are observed which represent the higher harmonics of the observed peak frequency.

3.2.3. *Case 3:* $\omega_A \neq \omega_B \neq 0$

In this sub-section, the lane formation dynamics of the 3-D PIP system is studied when external non-parallel oscillatory fields with different frequencies are applied to the system. For this, force $\boldsymbol{F}_A$, having field strength E_A, frequency ω_A, is applied along the z-direction, while another force $\boldsymbol{F}_B$ with field strength E_B, frequency ω_B is applied along the x-direction. The entire work is performed for $\omega_A \neq \omega_B \neq 0$.

https://doi.org/10.1017/S0022377823000387 Published online by Cambridge University Press

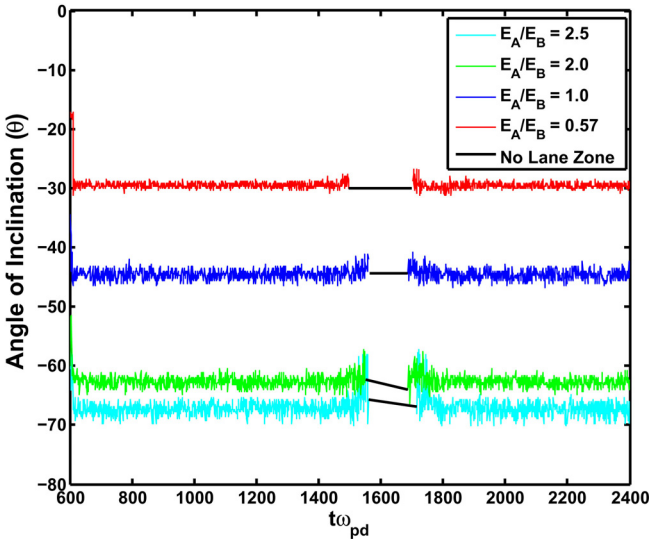

FIGURE 16. Angle of inclination 'θ' (in degree) versus $t\omega_{pd}$ plot of the 3-D PIP system with non-parallel oscillatory external fields. The black line is drawn later to indicate the region where there is a no lane state. External electric field is applied at the $t\omega_{pd} = 600$ time step where half of the PIP particles are drifting in the z-direction with force $\boldsymbol{F}_A = 200$, while the other half of the PIP particles are drifting in the x-direction with a varying force $\boldsymbol{F}_B = 80, 100, 200, 350$, such that $F_r = 2.5, 2.0, 1.0, 0.57$, respectively. The other parameters used are $\Gamma = 2.5$, $\rho = 0.245$ and $\omega_A = \omega_B = 0.001$.

In figure 18, the angle of inclination θ is plotted against $t\omega_{pd}$ for $E_A/E_B = 2.5$, $\omega_A = 0.001$ and $\omega_B = 0.01$, (i.e. $\omega_A < \omega_B$) along with the curve obtained using (2.1). The other parameters used are $\Gamma = 2.5$, $\rho = 0.245$ and $\beta = 0$ (see figure 18*a*), and a comparative study for $\beta = 1.0, 0$ (see figure 18*b*). Since, in most cases, the driving frequencies are comparable to the value of $\Delta t = 0.003$, performing simulations for very small values of $\Delta t = 0.0006$ led to the conclusion that $\Delta t = 0.003$ is small enough to study the dynamical property of the system. The associated results are provided in the Appendix. Figure 18(*a*) shows that the maximum and minimum values of θ, as predicted by using (2.1), are $[-90^\circ, 90^\circ]$, while the simulation does not exhibit the whole range of θ values as predicted by using (2.1) for the same set of parameters under use. Rather, the system goes into a disordered state when $|\theta|$ approaches the maximum or minimum θ value, and it stays in this region for a while before re-gaining a highly ordered lane state; however, this time the lane is rotated by 90°. Similar observations are recorded in the presence of a magnetic field also. In figure 18(*b*), a comparative plot for $\beta = 0$ and 1 is also shown.

To account for the formation and breaking of lanes, in figure 19(*a*), the order parameter with a gradient of θ ($\phi(\theta)$) is plotted against $t\omega_{pd}$, using the same set of parameters as used in figure 18. Here the colour bar indicates variation of θ with time; however, the results are shown in the absence of an external magnetic field. Here, the measurement of $\phi(\theta)$ is done after the application of the non-parallel forces at $t\omega_{pd} = 600$. As presented in figure 19(*a*), initially a peak is obtained at $t\omega_{pd} = 650$ with $\phi(\theta) = 0.57$. At this instant of time, the lanes are oriented at an angle $\theta = -63.65^\circ$, which is indicated by the blue spectrum of the colour bar. The order parameter is then reduced to a minimum of $\phi = 0.19$ at $t\omega_{pd} = 770$ and the system transits into a disordered state. Following this

https://doi.org/10.1017/S0022377823000387 Published online by Cambridge University Press

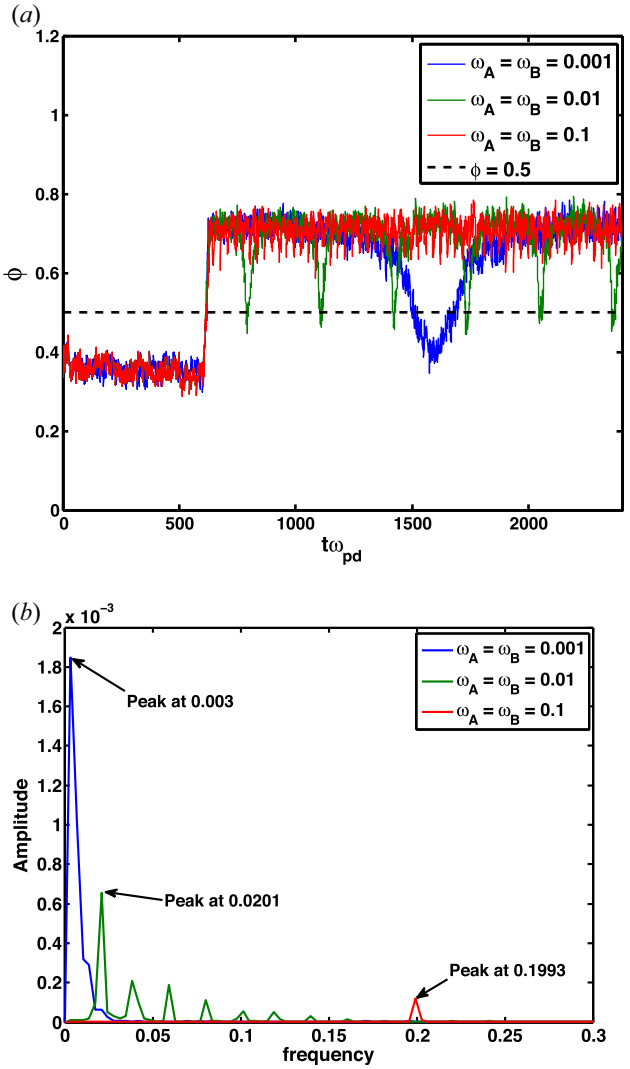

FIGURE 17. (*a*) Instantaneous order parameter (ϕ) versus $t\omega_{pd}$ plot for 3-D PIP system with non-parallel oscillatory fields $\boldsymbol{F}_A$ and $\boldsymbol{F}_B$ for $\omega_A = \omega_B = 0.001$, 0.01 and 0.1. (*b*) Single-sided Fourier transform of $\phi(t)$ shown in panel (*a*). The parameters used are $E_A = 200$, $E_B = 350$ $\Gamma = 2.5$ and $\rho = 0.245$.

disordered region, the system is again self-organised to form a lane state. However, the lanes formed is now rotated by approximately 90° and, in turn, a new crest is formed in the red spectrum of colour bar with its peak being at $t\omega_{pd} = 980$ with $\phi = 0.66$. This pattern of crests occurs repetitively throughout the simulation run. It is also noted that in between the flipping phases of lanes, there exists a period where the system remains in the no lane state for a longer duration of time from $t\omega_{pd} = 1390$ to 1750. As predicted by (2.1), the change in θ in this region is very rapid. The system is unable to adapt to this rapid change and responds by being in a no lane state during this time period. It is true for all cases of non-parallel time-varying external forces, whenever θ is expected to vary rapidly, a no lane state is followed. In figure 19(*b*), simulation snapshots recorded at

https://doi.org/10.1017/S0022377823000387 Published online by Cambridge University Press

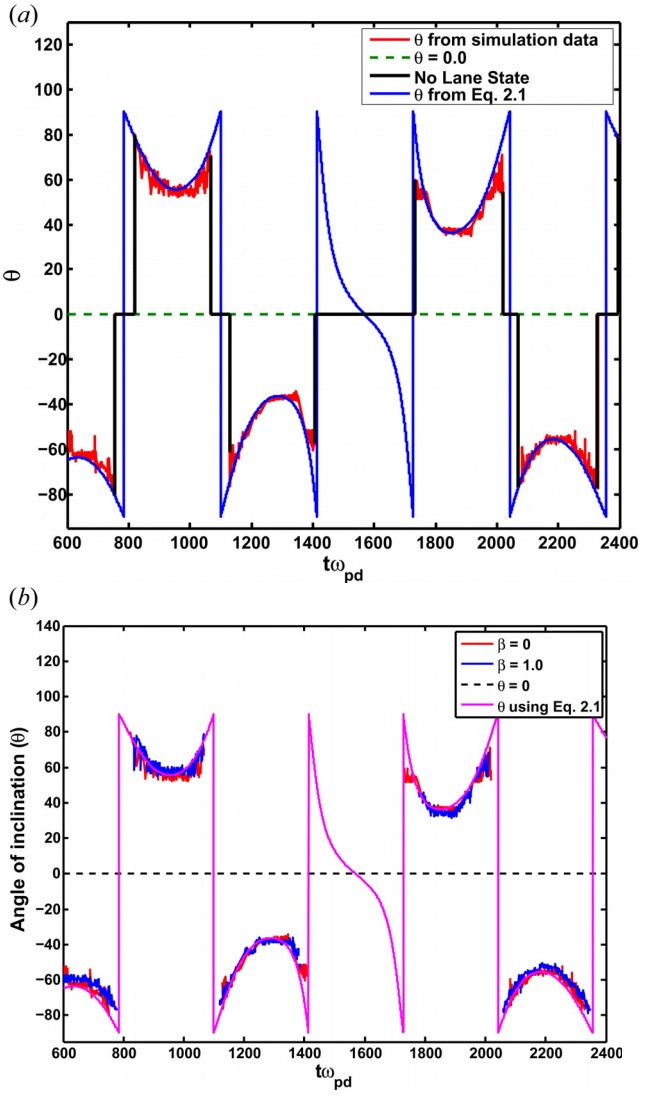

FIGURE 18. Angle of inclination 'θ' (in degree) versus $t\omega_{pd}$ plot of the 3-D PIP system with non-parallel oscillatory external fields of unequal frequency ($\omega_A \neq \omega_B$) for (*a*) $\beta = 0$ and (*b*) comparative plot for $\beta = 1.0$ and 0. An external electric field is applied at the $t\omega_{pd} = 600$ time step, where, half of the PIP particles are drifting in the z-direction with force $\boldsymbol{F}_A = 200$ with $\omega_A = 0.001$, while the other half of the PIP particles are drifting in the x-direction with force $\boldsymbol{F}_B = 80$ having frequency $\omega_B = 0.01$. The other parameters used are $\Gamma = 2.5$ and $\rho = 0.245$.

$t\omega_{pd} = 980$, 1320, 1890 and 2210, correspond to the situations mentioned in figure 19(*a*). Here, the snapshots are plotted such that the 3-D states are visualised. To achieve this, the particles are plotted having a gradient in transparency along the y-axis, where particles at $Y = -L_y/2$ have maximum transparency and particles at $Y = +L_y/2$ have the least transparency, i.e. are solid. The transparent layers make it easier to view the particles at the back of the simulation box. It is to be noted that transparency is associated only with the plotting of the particles. It does not change any physical property of the system under

https://doi.org/10.1017/S0022377823000387 Published online by Cambridge University Press

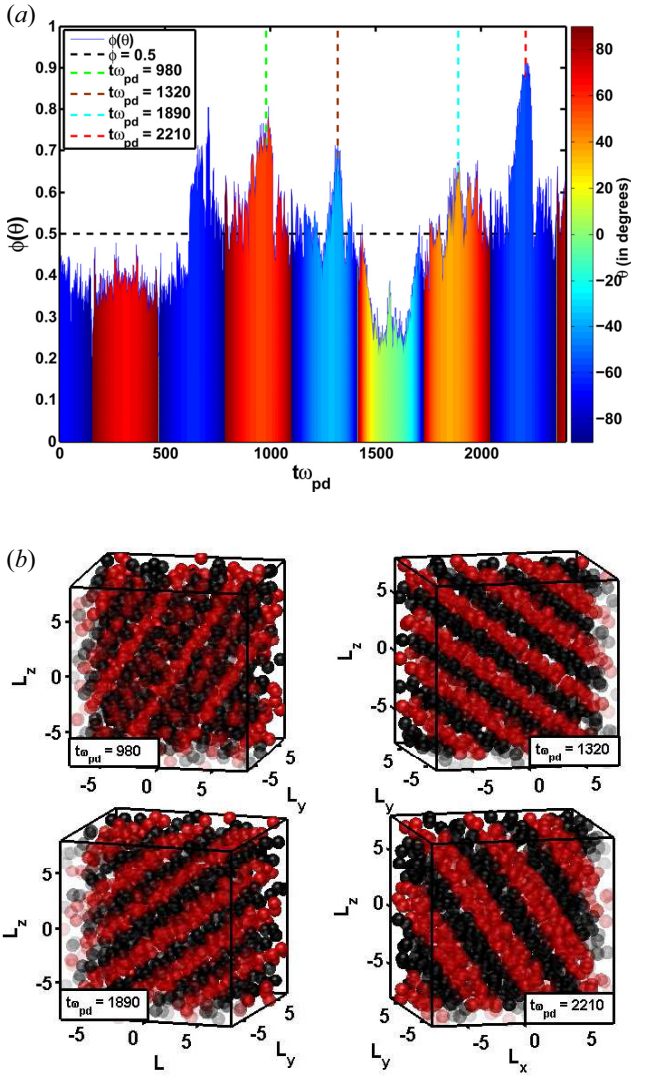

FIGURE 19. (*a*) Order parameter with gradient of $\theta(\phi(\theta))$ against $t\omega_{pd}$ in the presence of a non-parallel oscillatory external electric field ($\omega_A = 0.001$ and $\omega_B = 0.01$) with field strengths $E_A = 200$ and $E_B = 80$. The colour bar indicating the angle of inclination in degrees at which the measurement is taken for any instant of time. (*b*) Corresponding simulation snapshot of the 3-D PIP system representing the 3-D states taken at $t\omega_{pd} = 980$, 1320, 1890, 2210. The other parameters used are $\Gamma = 2.5$, $\rho = 0.24$ and $\beta = 0.0$.

study. The first snapshot taken at $t\omega_{pd} = 980$ clearly is in a self-organised state with its lanes forming an angle of inclination $\theta = 56.24^\circ$, which is then followed by a disordered state. The next snapshot taken at $t\omega_{pd} = 1320$ shows a lane state; however, the lanes are rotated to the negative domain with a new angle of inclination value $\theta = -37.5^\circ$. The next two snapshots taken at $t\omega_{pd} = 1890$ and 2210 show flipping of lanes with $\theta = +38.16^\circ$ and -56.03°, respectively.

In figure 20(*a*), the time variation of the angle of inclination (θ) is shown for $E_A/E_B = 2.5$, $\omega_A = 0.01$ and $\omega_B = 0.001$. Here, the frequencies of the forces $\boldsymbol{F}_A$ and

https://doi.org/10.1017/S0022377823000387 Published online by Cambridge University Press

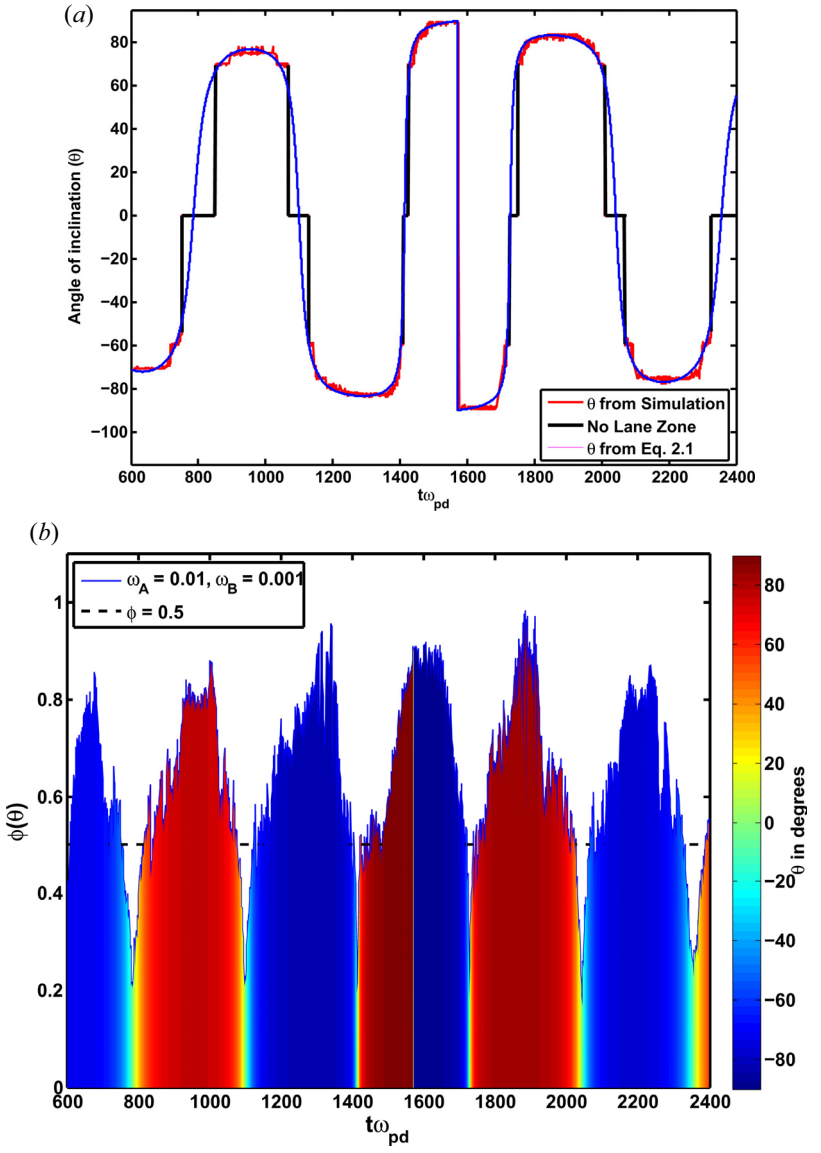

FIGURE 20. (*a*) Time variation of angle of inclination 'θ' (in degree). (*b*) Order parameter with gradient of $\theta(\phi(\theta))$ against $t\omega_{pd}$ in the presence of a non-parallel oscillatory external electric field ($\omega_A = 0.01$ and $\omega_B = 0.001$) with field strength $E_A = 200$ and $E_B = 80$. The colour bar indicating the angle of inclination in degrees at which the measurement is taken for any instant of time. The other parameters used are $\Gamma = 2.5$, $\rho = 0.24$ and $\beta = 0.0$.

$\boldsymbol{F}_B$ are interchanged such that $\omega_A > \omega_B$. It is observed that the pattern of the θ curve is changed. However, the flipping of lanes is observed even after interchanging ω_A and ω_B values. Upon performing extensive analysis, it is concluded that when $\omega_A < \omega_B$, the time variation of the angle of inclination takes the form shown in figure 18(*a*). However, when $\omega_A > \omega_B$, the angle of inclination variation takes the form shown in figure 20(*a*), where the amplitude of the oscillation is determined by the ratio of the electric field strengths i.e. E_A/E_B. In figure 20(*b*), the time variation of $\phi(\theta)$ is shown for the interchanged frequency

https://doi.org/10.1017/S0022377823000387 Published online by Cambridge University Press

case. It is observed that a tendency of spontaneous formation and breaking of lanes exist within the system under the influence of non-parallel forces when $\omega_A > \omega_B$; however, after every break of lanes, the new lanes are formed in an opposite domain of θ.

We finish by stating that lane formation is also expected to occur in 3-D PIP systems in the presence of both parallel and non-parallel forcing. As mentioned earlier, in general, non-parallel forcing can be realised by the crossing of two external fields like two electric fields, as used in our case of study. In the present case, the constituting species of the system avoid each other by forming lanes. Our set-up of non-parallel external electric forcing can be realised by visualising two crossing pedestrian lanes. Based on our results, tilted lanes are expected to form. Such phenomena are often responsible for various structures occurring in nature. Understanding and controlling such structures can have important technological implications. In some plasma processes, these structures could be desirable, adding to the outcome of the processes, whereas in other processes, it could be detrimental and hence undesirable. Our simulation results provide important insights into the controlling parameter range of one such structure formation which can be used to either mitigate or exploit this structure or lane formation in applications like determining the uniformity of plasma surface treatments or surface texturization to electrode erosion rates.

4. Conclusions

In this Part 2 of the work, we have presented a study of lane formation dynamics in a 3-D PIP system in the presence of non-parallel external electric forces both in the presence and absence of a magnetic field. Extensive Langevin dynamics simulation is performed using Open MP parallel code and it is observed that, as discussed in the companion paper Part 1 of the work, pattern formation is also exhibited by the PIP system in the presence of non-parallel forces. The conclusions drawn from Part 2 of the work are listed as follows.

(i) We observe that pattern formation in a PIP system is exhibited, which is independent of the orientation and direction of electric fields. Our set-up of non-parallel electric fields is realised by two crossing pedestrian lanes in which pedestrians are only moving in one direction.

(ii) As the main results, we find tilted lanes in the presence of non-parallel forces. The lanes are directed along the difference vector of the two applied fields. However, parallel lanes are observed on application of parallel forces, as discussed in Part 1 of the work.

(iii) The ratio of two externally applied electric field strengths greatly influences the angle of inclination of the lanes. With increasing $\frac{E_A}{E_B}$, the angle of inclination also increases. Here, E_A and E_B are the magnitude of the non-parallel electric forces F_A and F_B, respectively.

(iv) It is observed that the fluctuations in θ have a Gaussian distribution about the mean $\bar{\theta}$, with $\bar{\theta}$ being the accurate value of the angle of inclination for any particular case.

(v) Application of an oscillatory electric field paints a very different picture of the system. When one force is oscillatory and the other force is constant in nature ($i.e. \omega_A \neq 0, \omega_B = 0$), then the angle of inclination (θ) also oscillates within a range determined by (2.1). The range of oscillation of θ also increases with increasing E_A/E_B. Additionally, the frequency of oscillation of θ is found to be equal to the frequency of the applied external field and changes accordingly.

(vi) There is a tendency of repetitive breaking and formation of lanes at unequal interval, the frequency of which is different from that of the applied external field.

https://doi.org/10.1017/S0022377823000387 Published online by Cambridge University Press

(vii) When both applied forces are oscillating in nature and have the same frequencies (i.e. $\omega_A = \omega_B \neq 0$), the oscillation in θ disappears and θ becomes constant for a given E_A/E_B; however, $|\theta|$ increases with increasing E_A/E_B. Additionally, a repetitive lane breaking and formation is also observed in the lower frequency regime, the frequency of which is dependent on the frequency of the applied external forces; however, it is not equal to the driving frequency and may be generated by the system in response to the applied non-parallel forcing.

(viii) In the presence of oscillatory forces oscillating with different frequencies, a peculiar behaviour similar to a flipping of the lane orientation is noted, where the angle of inclination is changed by almost 90° in a very short interval of time in a recursive manner.

(ix) Two distinct patterns of time variation of the angle of inclination plot are observed depending on the ratio of ω_A/ω_B, and the amplitude of oscillations in θ are highly dependent on ω_A/ω_B. Also, in the absence of a magnetic field, the angle of inclination in any case can be determined satisfactorily by using (2.1).

(x) The effect of the magnetic field on the lane formation dynamics is also studied. Interestingly, the magnetic field contributed towards the order of the lanes. It is also observed that the magnetic field reduces the angle of inclination θ and this change is more at higher E_A/E_B values.

(xi) Furthermore, as concluded in Part 1 of the companion paper, here, in presence of non-parallel forces, a drift of lanes in a direction perpendicular to both applied electric and magnetic field is also observed.

A study on lane formation dynamics in a 3-D PIP system under the influence of external parallel (Part 1 of the companion paper (Prajapati *et al.* 2023)) and non-parallel forces both in the presence and absence of a magnetic field is reported here. Our study may provide insights to pattern formation in a 3-D regime and will help to understand plasma dynamics.

Acknowledgements

V.K.P. and S.B. would like to thank Professor R. Ganesh for his productive discussions. The authors would also like to acknowledge Institute for Plasma Research (IPR), Bhat, Gandhinagar, for allowing use of the HCP cluster at IPR. All authors thank the Editor Dr Edward Thomas for accepting the manuscript and the referees for their advice in evaluating this article.

Editor Edward Thomas Jr. thanks the referees for their advice in evaluating this article.

Funding

This research work is supported under INSPIRE Program by Department of Science and Technology (DST) (V.K.P., sanctioned no. DST/INSPIRE Fellowship/2019/IF190899, dated 29/10/2021).

Declaration of interests

The authors report no conflict of interest.

Author contributions

All authors contributed equally in preparing the theoretical model, in performing the simulations, analysing data, reaching conclusions and writing the paper.

https://doi.org/10.1017/S0022377823000387 Published online by Cambridge University Press

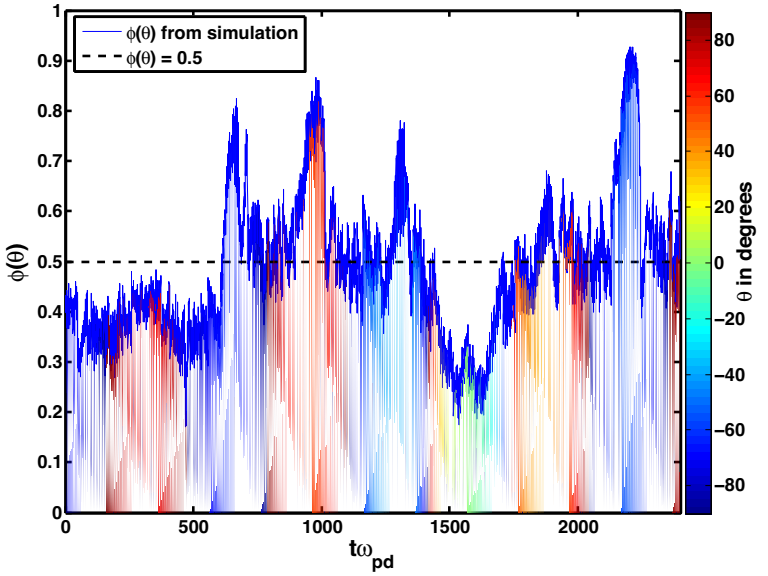

FIGURE 21. Angle of inclination versus $t\omega_{pd}$ plot of the 3-D PIP system with non-parallel oscillatory external fields of unequal frequency ($\omega_A = 0.001$ and $\omega_B = 0.01$) for $\Delta t = 0.0006$. The other parameters used are $E_A/E_B = 2.5$, $\Gamma = 2.5$ and $\rho = 0.245$.

Data availability statement

The data that support the findings of this study are available from the corresponding author upon reasonable request.

Appendix

In figure 21, the time variation of the angle of inclination (θ) is shown for $\Delta t = 0.0006$. It is observed that there is almost no difference with the profile of the curve for $\Delta t = 0.003$ shown in figure 19(a) for the same parameters. In response to the different time-varying forces applied to the system, the system generates a variety of small and large frequencies. Figure 21 is crucial to characterise these frequencies as system generated rather than a numerical inaccuracy. The overall behaviour of the system remains the same for both $\Delta t = 0.003$ and 0.0006, which indicates that $\Delta t = 0.003$ is small enough to predict the dynamical properties of the system.

REFERENCES

ABURDZHANIIA, G.D., MIKHAILOVSKII, A.B., ONISHCHENKO, O.G., SHARAPOV, S.E. & CHURIKOV, A.P. 1984 Electromagnetic vortices in a plasma. In *Nonlinear and Turbulent Processes in Physics* (ed. R.Z. Sagdeev), p. 1. Harwood Academic Publishers.

BARUAH, S., PRAJAPATI, V.K. & GANESH, R. 2021*a* Lane dynamics in pair-ion plasmas: effect of obstacle and geometric aspect ratio. *J. Plasma Phys*. **87** (6), 905870601.

BARUAH, S., SARMA, U. & GANESH, R. 2021*b* Effect of external magnetic field on lane formation in driven pair-ion plasmas. *J. Plasma Phys*. **87** (2), 905870202.

BRUGGEMAN, P. & LEYS, C. 2009 Non-thermal plasmas in and in contact with liquids. *J. Phys. D: Appl. Phys*. **42** (5), 053001.

DZUBIELLA, J., HOFFMANN, G.P. & LÖWEN, H. 2002 Lane formation in colloidal mixtures driven by an external field. *Phys. Rev.* E **65**, 021402.

https://doi.org/10.1017/S0022377823000387 Published online by Cambridge University Press

GLANZ, T. & LÖWEN, H. 2012 The nature of the laning transition in two dimensions. *J. Phys.: Condens. Matter* **24** (46), 464114.

HYNNINEN, A.-P., LEUNISSEN, M.E., VAN BLAADEREN, A. & DIJKSTRA, M. 2006 Cuau structure in the restricted primitive model and oppositely charged colloids. *Phys. Rev. Lett*. **96**, 018303.

KONG, M.G., KROESEN, G., MORFILL, G., NOSENKO, T., SHIMIZU, T., VAN DIJK, J. & ZIMMERMANN, J.L. 2009 Plasma medicine: an introductory review. *New J. Phys*. **11** (11), 115012.

LEUNISSEN, M.E., CHRISTOVA, C.G., HYNNINEN, A.-P., ROYALL, C.P., CAMPBELL, A.I., IMHOF, A., DIJKSTRA, M., VAN ROIJ, R. & VAN BLAADEREN, A. 2005 Ionic colloidal crystals of oppositely charged particles. *Nature* **437** (7056), 235–240.

LICHTENBERG, S., NANDELSTÄDT, D., DABRINGHAUSEN, L., REDWITZ, M., LUHMANN, J. & MENTEL, J. 2002 Observation of different modes of cathodic arc attachment to hid electrodes in a model lamp. *J. Phys. D: Appl. Phys*. **35** (14), 1648.

OSTRIKOV, K.K., CVELBAR, U. & MURPHY, A.B. 2011 Plasma nanoscience: setting directions, tackling grand challenges. *J. Phys. D: Appl. Phys*. **44** (17), 174001.

PODVIGINA, O.M. 2006 Magnetic field generation by convective flows in a plane layer. *Eur. Phys. J.* B **50**, 639–652.

PRAJAPATI, V.K., BARUAH, S. & GANESH, R. 2023 Lane formation in 3D driven pair-ion plasmas: I Parallel External Forcing. *J. Plasma Phys.* **89**, 905890301. doi:10.1017/S0022377823000375

SARMA, U., BARUAH, S. & GANESH, R. 2020 Lane formation in driven pair-ion plasmas. *Phys. Plasmas* **27**, 012106.

SUN, Z. & ALWAHABI, Z. 2022 Beam-crossing configuration to control plasma position, improve spatial resolution, and enhance emissions in single-pulse, laser-induced breakdown spectroscopy in gases. *Appl. Opt*. **61** (2), 316–323.

TRAYLOR, M.J., PAVLOVICH, M.J., KARIM, S., HAIT, P., SAKIYAMA, Y., CLARK, D.S. & GRAVES, D.B. 2011 Long-term antibacterial efficacy of air plasma-activated water. *J. Phys. D: Appl. Phys*. **44** (47), 472001.

TRELLES, J.P. 2013 Computational study of flow dynamics from a dc arc plasma jet. *J. Phys. D: Appl. Phys*. **46** (25), 255201.

YANG, G. & HEBERLEIN, J. 2007 Instabilities in the anode region of atmospheric pressure arc plasmas. *Plasma Sources Sci. Technol*. **16** (4), 765.